Evolution of Antibody Immunity to SARS-CoV-2

Christian Gaebler[1*], Zijun Wang[1*], Julio C. C. Lorenzi[1*], Frauke Muecksch[2*], Shlomo Finkin[1*], Minami Tokuyama[3*], Mark Ladinsky[4*], Alice Cho[1*], Mila Jankovic[1*], Dennis Schaefer-Babajew[1*], Thiago Y. Oliveira[1*], Melissa Cipolla[1*], Charlotte Viant[1], Christopher O. Barnes[4], Arlene Hurley[5], Martina Turroja[1], Kristie Gordon[1], Katrina G. Millard[1], Victor Ramos[1], Fabian Schmidt[2], Yiska Weisblum[2], Divya Jha[3], Michael Tankelevich[3], Jim Yee[6], Irina Shimeliovich[1], Davide F. Robbiani[7], Zhen Zhao[6], Anna Gazumyan[1], Theodora Hatziioannou[2], Pamela J. Bjorkman[4], Saurabh Mehandru[3,#], Paul D. Bieniasz[2,8,#], Marina Caskey[1,#], Michel C. Nussenzweig[1,8,#]

[1]Laboratory of Molecular Immunology, The Rockefeller University, New York, NY 10065, USA

[2]Laboratory of Retrovirology, The Rockefeller University, New York, NY 10065, USA

[3] Division of Gastroenterology, Department of Medicine, Icahn School of Medicine at Mount Sinai, New York, NY 10029, USA.

[4] Division of Biology and Biological Engineering, California Institute of Technology, Pasadena, CA, USA.

[5]Hospital Program Direction, The Rockefeller University, New York, NY 10065, USA

Hospital Clinical Research Office, The Rockefeller University, New York, NY 10065, USA

[6]Department of Pathology and Laboratory Medicine, Weill Cornell Medicine, New York, NY, USA

[7] Institute for Research in Biomedicine, Università della Svizzera italiana, Bellinzona, Switzerland.

[8]Howard Hughes Medical Institute

24

25 *Equal contribution

26

27 #Send correspondence to Saurabh Mehandru: saurabh.mehandru@mssm.edu, Paul D. Bieniasz:
28 pbieniasz@rockefeller.edu, Marina Caskey: mcaskey@rockefeller.edu, or Michel C.
29 Nussenzweig: nussen@rockefeller.edu

30

SARS-CoV-2 has infected 47 million individuals and is responsible for over 1.2 million deaths to date. Infection is associated with development of variable levels of antibodies with neutralizing activity that can protect against infection in animal models. Antibody levels decrease with time, but the nature and quality of the memory B cells that would be called upon to produce antibodies upon re-infection has not been examined. Here we report on the humoral memory response in a cohort of 87 individuals assessed at 1.3 and 6.2 months after infection. We find that IgM, and IgG anti-SARS-CoV-2 spike protein receptor binding domain (RBD) antibody titers decrease significantly with IgA being less affected. Concurrently, neutralizing activity in plasma decreases by five-fold in pseudotype virus assays. In contrast, the number of RBD-specific memory B cells is unchanged. Memory B cells display clonal turnover after 6.2 months, and the antibodies they express have greater somatic hypermutation, increased potency and resistance to RBD mutations, indicative of continued evolution of the humoral response. Analysis of intestinal biopsies obtained from asymptomatic individuals 3 months after COVID-19 onset, using immunofluorescence, electron tomography or polymerase chain reaction, revealed persistence of SARS-CoV-2 in the small bowel of 7 out of 14 volunteers. We conclude that the memory B cell response to SARS-CoV-2 evolves between 1.3 and 6.2 months after infection in a manner that is consistent with antigen persistence.

Antibody responses to SARS-CoV-2 were initially characterized in a cohort of COVID-19-convalescent individuals approximately 40 days (1.3 months) after infection [1]. Between 31 August and 16 October 2020, 100 participants returned for a 6-month follow-up study visit. Although initial criteria allowed enrollment of close contacts of individuals diagnosed with RT-PCR confirmed SARS-CoV-2 infection [1], 13 of the contacts did not seroconvert and were excluded from further analyses. The remaining 87 participants with RT-PCR–confirmed COVID-19 diagnosis and/or seroconversion returned for analysis approximately 191 days (6.2 months, range: 165-223 days) after the onset of symptoms. In this cohort, symptoms lasted for a median of 12 days (0–44 days) during the acute phase, and 10 (11%) of the participants were hospitalized. Consistent with other reports [2,3], 38 (44%) of the participants reported persistent long-term symptoms attributable to COVID-19 (Methods and Supplementary Tables 1 and 2). The duration and severity of symptoms during acute disease was significantly greater among participants with persistent post-acute symptoms at the second study visit (Extended Data Fig. 1m-o). Importantly, all 87 participants tested negative for SARS-CoV-2 at the 6-month follow-up study visit using an approved saliva-based PCR assay (Methods). Participant demographics and clinical characteristics are shown in Supplementary Tables 1,2.

Antibody reactivity in plasma to RBD and nucleoprotein (N) was measured by validated serological assays [1,4,5]. Two anti-RBD assays were strongly correlated (anti-RBD IgG and IgM ELISA/Pylon-IgG and IgM at 1.3 months, $r=0.9200$ and $r=0.7543$, $p < 0.0001$, respectively. Extended Data Fig 2). The IgM, IgG and IgA anti-RBD antibodies in plasma decreased significantly between 1.3 and 6.2 months (Fig. 1a-c). However, the drop in RBD-binding activity differed significantly by isotype, IgM showed the greatest decrease in anti-RBD reactivity (53%),

73 followed by IgG (33%) while IgA decreased by only 15% (Fig. 1e). In all cases the magnitude of
74 the decrease was inversely proportional to and directly correlated with the initial antibody levels
75 such that individuals with higher initial levels showed greater relative changes (Fig. 1f-i). In
76 contrast, the Roche anti-N assay[5] showed a small but significant increase (19%) in reactivity
77 between the two time points that did not correlate with IgA anti-RBD ELISAs and was modestly
78 correlated with IgM at 1.3 months and IgG anti-RBD reactivity at both time points, respectively
79 (Fig. 1d and Extended Data Fig. 2i-n). Notably, individuals with persistent post-acute symptoms
80 had significantly higher anti-RBD IgG and anti-N antibody levels at both study visits (Extended
81 Data Fig. 1a-j).
82
83 Plasma neutralizing activity was measured using an HIV-1 virus pseudotyped with the SARS-
84 CoV-2 spike protein[1,6]. Consistent with other reports the geometric mean half-maximal
85 neutralizing titer (NT_{50}) in this group of 87 participants was 401 and 78 at 1.3 and 6.2 months,
86 respectively, representing a five-fold decrease (Fig. 1j-k)[7,8]. Neutralizing activity was directly
87 correlated with the IgG anti-RBD ELISA measurements (Extended data Fig. 2o-p). Moreover, the
88 absolute magnitude of the decrease in neutralizing activity was inversely proportional to and
89 directly correlated with the neutralizing activity at the earlier time point (Fig. 1l). We conclude
90 that antibodies to RBD and plasma neutralizing activity decrease significantly but remain
91 detectable 6 months after infection with SARS-CoV-2 in the majority of individuals.
92
93 Whereas plasma cells are the source of circulating antibodies, memory B cells contribute to recall
94 responses. To identify and enumerate the circulating SARS-CoV-2 memory B cell compartment
95 we used flow cytometry to isolate individual B lymphocytes with receptors that bound to RBD [1]

(Fig. 2a and b, and Extended data Fig. 3). Notably, the percentage of RBD-binding memory B cells increased marginally between 1.3 and 6.2 months in 21 randomly selected individuals (Fig. 2b).

To determine whether there were changes in the antibodies produced by memory B cells after 6.2 months, we obtained 532 paired antibody heavy and light chains from the same 6 individuals that were examined at the earlier time point [1] (Supplementary Table 3). There was no significant difference in IGV gene representation at the two time points, including the over-representation of the *IGHV3-30* and *3-53* gene segments [1,9-14] (Extended data Fig. 4). In keeping with this observation, and similar to the earlier time point, antibodies that shared the same IGHV and IGLV genes comprised 8.6% of all sequences in different individuals (Extended data Fig. 5a). As might be expected, there was a small but significant overall increase in the percentage of IgG-expressing anti-RBD memory cells, from 47% to 57% ($p=0.011$, Extended data Fig. 5b-d). Consistent with the fractional increase in IgG memory cells, the extent of somatic hypermutation for both IGH and IGL differed significantly in all 6 individuals between the two time points. Whereas the average number of nucleotide mutations in IGH and IGL was only 4.2 and 2.8 at the first time point, these values were increased to 11.7 and 6.5 at the second time point ($p<0.0001$, Fig. 2c and Extended data Fig. 6). In contrast, the overall average IGH and IGL CDR3 length and hydrophobicity were unchanged (Extended data Fig. 7).

Similar to the earlier time point, we found expanded clones of memory B cells at 6.2 months including 23 that appeared at both time points. However, expanded clones accounted for only 12.4% of all antibody sequences after 6.2 months compared to 32% after 1.3 months ($p = 0.0225$,

Fig. 2d-e). In addition, the overall clonal composition of the memory compartment differed at the two time points in all individuals examined (Fig. 2d). Forty-three expanded clones that were present at the earlier time point were not detectable after 6.2 months while 22 new expanded clones appeared. In addition, the relative distribution of clones that appeared at both time points also varied. For example, the dominant clones in COV21 and COV57 representing 9.0% and 16.7% of all sequences, respectively, were reduced to 1.1% and 1.9% of all sequences after 6.2 months (Fig. 2d and Supplementary Table 3). We conclude that while the magnitude of the RBD-specific memory B cell compartment is conserved between 1.3 and 6.2 months after SARS-CoV-2 infection, there is significant clonal turnover and antibody sequence evolution, consistent with prolonged germinal center reactions.

One hundred and twenty-two representative antibodies from the 6.2-month time point were tested for reactivity to RBD (Supplementary Table 4). The antibodies that were evaluated included: (1) 49 that were randomly selected from those that appeared only once; (2) 23 that appeared as singles at both 1.3 and 6.2 months; (3) 23 representatives of newly appearing expanded clones; (4) 27 representatives of expanded clones appearing at both time points. One hundred and fifteen of 122 of the antibodies bound to RBD indicating that flow cytometry efficiently identified B cells producing anti-RBD antibodies (Fig. 3a and Supplementary Tables 4 and 5). Taking all antibodies together, the mean ELISA EC_{50} was not significantly different at the two time points (Fig. 3a, Supplementary Table 4 and [1]). However, comparison of the antibodies that were present at both time points revealed a significant improvement of the EC_{50} after 6.2 months ($p= 0.0227$, Fig. 3b and Extended data Fig.8a).

142 To determine whether the antibodies expressed by memory B cells at the late time point also
143 showed altered breadth, we compared them to earlier clonal relatives in binding assays using
144 control and mutant RBDs: The mutations E484K and Q493R[15] were selected for resistance to class
145 2 antibodies such as C144 and C121 that bind directly to the ACE2 interaction ridge in the RBD
146 [1,16-18] while R346S, N439K, and N440K were selected for resistance to class 3 antibodies such as
147 C135 that do not directly interfere with ACE2 binding [1,15-18] (Fig.3c). In addition, V367F, A475V,
148 S477N, and V483A represent circulating variants that confer complete or partial resistance to class
149 1 and 2 antibodies [15,16,19] (Fig. 3c). Out of 52 antibody clonal pairs appearing at both time points,
150 43 (83%) showed overall increased binding to mutant RBDs at the 6.2-month time point (Extended
151 data Fig. 8b-k, Supplementary Table 5). For example, C144, an antibody recovered at the 1.3-
152 month time point, was unable to bind to Q493R or E484K RBDs, but all 4 of its 6.2-month clonal
153 derivatives bound to Q493R, and one also showed binding to E484K (Fig. 3d). Overall, the most
154 pronounced increase in binding occurred for RBD mutations in amino acid positions such as E484,
155 Q493, N439, N440 and R346 that are critical for binding of class 2 and 3 antibodies [15,16] (Fig. 3e,
156 Extended data Fig. 8b-k and Supplementary Table 5).
157
158 Next, all 122 antibodies from the 6.2 month time point were tested for activity in a pseudotyped
159 SARS-CoV-2 neutralization assay [1,6] (Fig. 4a, Supplementary Table 6). Consistent with RBD
160 binding assays, the mean neutralization IC_{50} values were not significantly different at the two time
161 points when all antibodies were compared (Fig. 4a and [1]). However, comparison of the antibodies
162 that were present at both time points revealed a significant improvement of the IC_{50} values at 6.2
163 months ($p=0.0003$, Fig. 4b and Extended data Fig. 9a).
164

To determine whether the antibodies exhibiting altered RBD binding also show increased neutralizing breadth, we tested 5 representative antibody pairs recovered at the two time points against HIV-1 viruses pseudotyped with E484G, Q493R, and R346S mutant spike proteins (Fig. 4c, Supplementary Table 6). Notably, the Q493R and E484G pseudotyped viruses were resistant to neutralization by C144; in contrast, its 6.2-month clonal derivative C051 neutralized both variants with IC_{50} values of 4.7 and 3.1 ng/ml respectively (Fig. 4c-d). Similarly, R346S pseudotyped viruses were resistant to C032, but a 6.2-month clonal derivative C080 neutralized this variant with an IC_{50} of 5.3 ng/ml (Fig. 4c, Extended data Fig. 9b-f). Consistent with the observed changes in binding and neutralizing activity several late-appearing antibodies (e.g. C051) had acquired mutations directly in or adjacent to the RBD-binding paratope (Fig. 4e, Extended data Fig. 10). We conclude that memory B cells that evolved during the observation period express antibodies with increased neutralizing potency and breadth.

Antibody evolution occurs by somatic mutation and selection in germinal centers wherein antigen can be retained in the form of immune complexes on the surface of follicular dendritic cells for prolonged periods of time. Residual virus in tissues represents another potential source of antigen. SARS-CoV-2 replicates in ACE2-expressing cells in the lungs, nasopharynx and small intestine [20-23], and viral RNA has been detected in stool samples even after the virus is cleared from the nasopharynx [24-26]. To determine whether there might be antigen persistence in the intestine after resolution of clinical illness, we obtained biopsies from the upper and lower gastrointestinal (GI) tract of 14 individuals, an average of 4 months (range 2.8-5.5 months) after initial SARS-CoV-2 diagnosis (Supplementary Table 7). Clinically approved nasopharyngeal swab PCR assays were negative in all 14 individuals at the time of biopsy. However, biopsy samples from 3 of the 14

188 participants produced PCR amplicons that were sequence verified as SARS-CoV-2 (Methods and
189 Supplementary Table 7). Immunostaining was performed to determine whether viral protein was
190 also detectable in upper and lower GI tract, with de-identified biopsies from individuals pre-dating
191 the pandemic (n=10) serving as controls. ACE2 and SARS-CoV-2 N protein was detected in
192 intestinal enterocytes in 5 of 14 individuals but not in historic control samples (Fig. 5a-d, Extended
193 data Fig. 11,12 and 13, and Supplementary Table 7). When detected, immunostaining was
194 sporadic, patchy, exclusive to the intestinal epithelium and not associated with inflammatory
195 infiltrates (Extended data Fig. 11,12).
196
197 Detection of SARS-CoV-2 RNA and N protein could represent defective viral particles and/or
198 infected cell debris. To determine whether viral particles were present we used electron
199 tomography to examine a tissue sample from one of the individuals who was positive by
200 immunofluorescence (Fig. 5e-j). Particles with typical SARS-CoV-2 morphologies were found
201 within intracellular membrane-enclosed vesicles consistent with coronavirus exit compartments in
202 terminal ileum apical epithelial cells (Fig. 5e-h), suggesting the presence of intact virions. Particles
203 were also found in vesicles in apical epithelial cells of the duodenum, although there were fewer
204 and less densely-populated vesicles observed (Fig. 5i-j).
205
206 Neutralizing antibodies to SARS-CoV-2 develop in most individuals after infection but decay with
207 time [7,8,27-31]. These antibodies are effective in prevention and therapy in animal models and are
208 likely to play a role in protection from re-infection in humans [32]. Although there is a significant
209 drop in plasma neutralizing activity between 1.3 and 6.2 months, antibody titers remain measurable
210 in most individuals [7,8,27-30,33].

Neutralizing monoclonal antibodies obtained from individuals during the early convalescence period showed remarkably low levels of somatic mutations that some investigators attributed to defects in germinal center formation [9,10,12,34-37]. Our data indicate that the anti-SARS-CoV-2 memory B cell response evolves during the first 6 months after infection, with accumulation of Ig somatic mutations, and production of antibodies with increased neutralizing breadth and potency. Persistent antibody evolution occurs in germinal centers and requires that B cells are exposed to antigen trapped in the form of immune complexes on follicular dendritic cells [38]. This form of antigen can be long-lived because follicular dendritic cells do not internalize immune complexes. In addition, even small amounts of persistent viral replication could contribute antigen to fuel antibody evolution. The observation that SARS-CoV-2 remains detectable in the small intestinal epithelium even 3 months after infection is consistent with the relative persistence of anti-RBD IgA antibodies and continued antibody evolution. However, the prevalence, clinical significance, and potential infectivity of residual SARS-CoV-2 in intestinal enterocytes remain to be determined.

Memory responses are responsible for protection from re-infection and are essential for effective vaccination. The observation that memory B cell responses do not decay after 6.2 months, but instead continue to evolve, is strongly suggestive that individuals who are infected with SARS-CoV-2 could mount a rapid and effective response to the virus upon re-exposure.

Figures

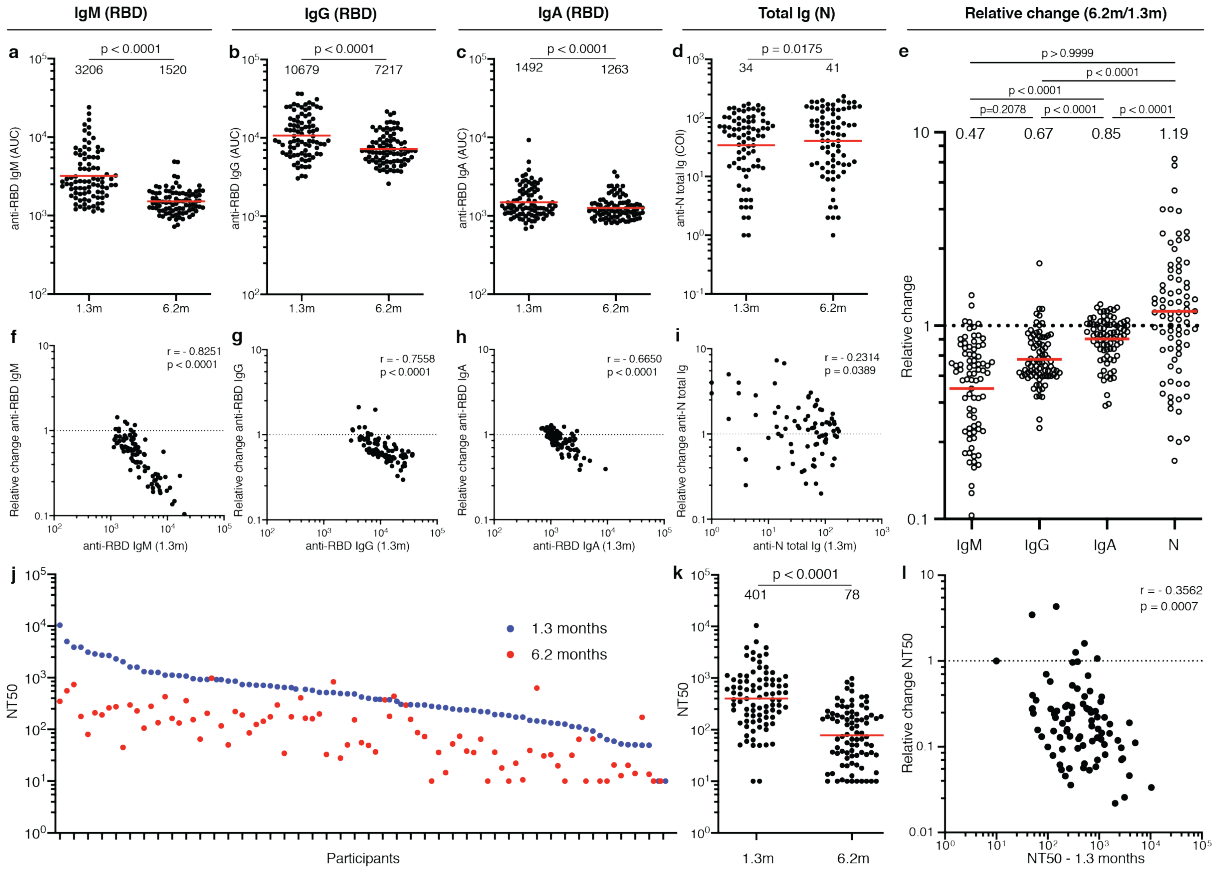

Fig. 1: Plasma antibody dynamics against SARS-CoV-2.

a–**d**, Results of serological assays measuring plasma reactivity to RBD (**a**,**b**,**c**) and N protein (**d**) at the initial 1.3 and 6.2 month follow-up visit, respectively. **a**, Anti-RBD IgM. **b**, Anti-RBD IgG. **c**, Anti-RBD IgA **d**, Anti-N total antibodies. The normalized area under the curve (AUC) values for 87 individuals and Cut-off Index (COI) values for 80 individuals are shown in **a,b,c** and **d** for both time points, respectively. Positive and negative controls were included for validation [1]. **e**, Relative change in plasma antibody levels between 1.3 and 6.2 months for anti-RBD IgM, IgG, IgA and anti-N total Ig, respectively. **f-i,** Relative change in antibody levels between 1.3 and 6.2

243 months plotted against the corresponding antibody levels at 1.3 months. **f**, Anti-RBD IgM. r = -
244 0.83, p <0.0001. **g**, Anti-RBD IgG. r = -0.76, p <0.0001. **h**, Anti-RBD IgA. r = -0.67, p <0.0001.
245 **i**, Anti-N total antibodies. r = -0.23, p = 0.039. **j.** Ranked average half-maximal inhibitory plasma
246 neutralizing titer (NT50) at 1.3 months (blue) and 6.2 months (red) for the 87 individuals studied.
247 **k.** Graph shows NT50 for plasma collected at 1.3 and 6.2 months p <0.0001. **l.** Relative change in
248 plasma neutralizing titers between 1.3 and 6.2 months plotted against the corresponding titers at
249 1.3 months. For **a**-**e**, **k** plotted values and horizontal bars indicate geometric mean. Statistical
250 significance was determined using Wilcoxon matched-pairs signed rank test in **a-d**, **k** and
251 Friedman with Dunn's multiple comparison test in **e**. The *r* and *p* values in **f** – **I** and **l** were
252 determined by two-tailed Spearman's correlations.

253

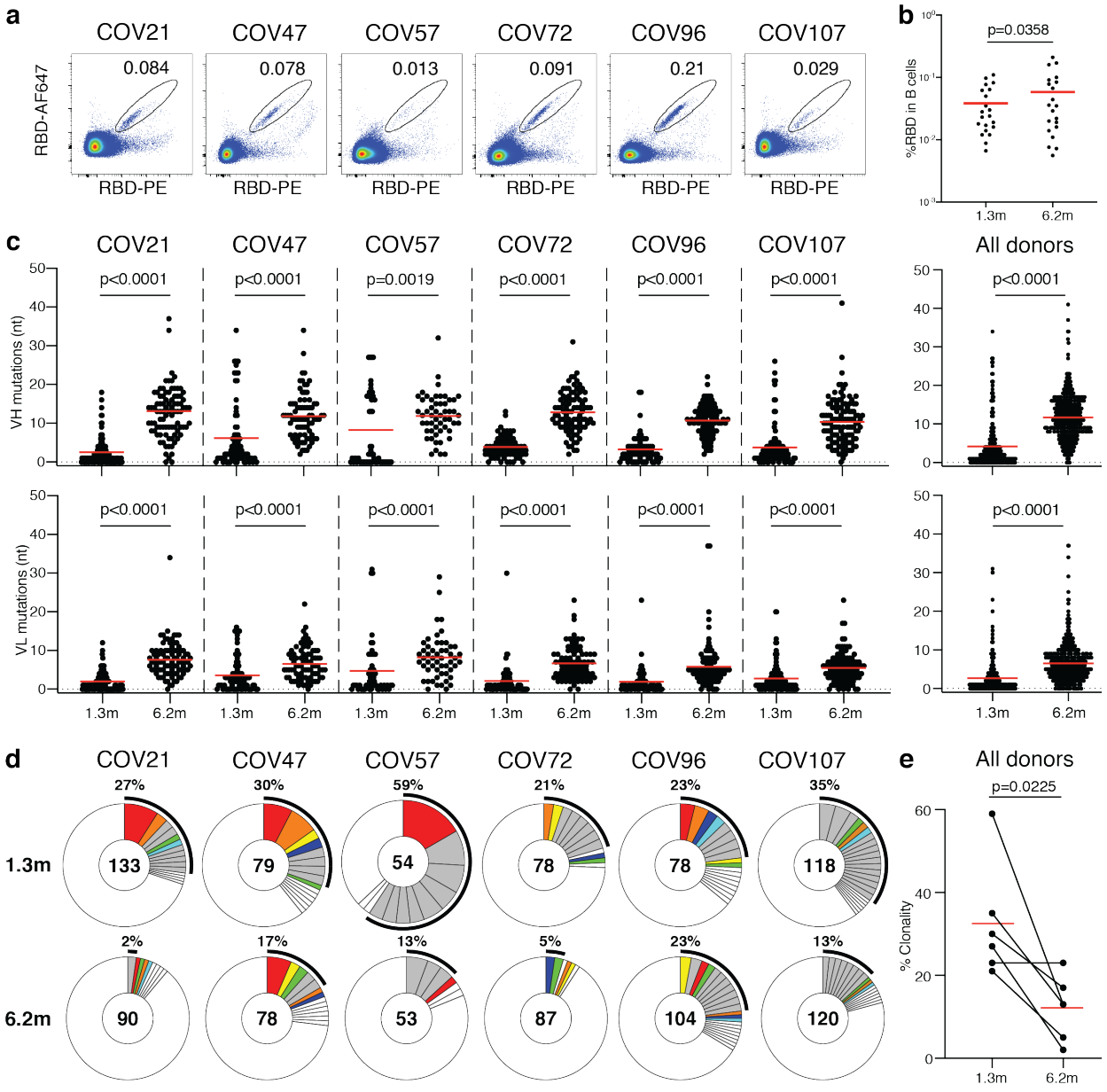

Fig. 2: Anti-SARS-CoV-2 RBD antibody sequences.

a, Representative flow cytometry plots showing dual AlexaFluor-647–RBD- and PE–RBD-binding B cells for six study individuals (gating strategy is in Extended Data Fig.3). Percentage of antigen-specific B cells is indicated. **b.** As in **a.** graph summarizes %RBD binding memory B cells in samples obtained at 1.3 and 6.2 months from 21 randomly selected individuals. Red horizontal bars indicate geometric mean values. Statistical significance was determined using Wilcoxon

matched-pairs signed rank test. **c,** Number of somatic nucleotide mutations in the IGVH (top) and IGVL (bottom) in antibodies obtained after 1.3 or 6.2 months from the indicated individual or all donors (right). **d,** Pie charts show the distribution of antibody sequences from 6 individuals after 1.3 [1] (upper panel) or 6.2 months (lower panel). The number in the inner circle indicates the number of sequences analyzed for the individual denoted above the circle. Pie slice size is proportional to the number of clonally related sequences. The black outline indicates the frequency of clonally expanded sequences detected in each patient. Colored slices indicate persisting clones (same IGHV and IGLV genes and highly similar CDR3s) found at both timepoints in the same patient. Grey slices indicate clones unique to the timepoint. White slices indicate singlets found at both timepoints, while the remaining white area indicates sequences isolated once. **e.** Graph shows relative clonality at both time points timepoints. Red horizontal bars indicate mean values. Statistical significance was determined using two-tailed Mann–Whitney U-tests or paired t-test.

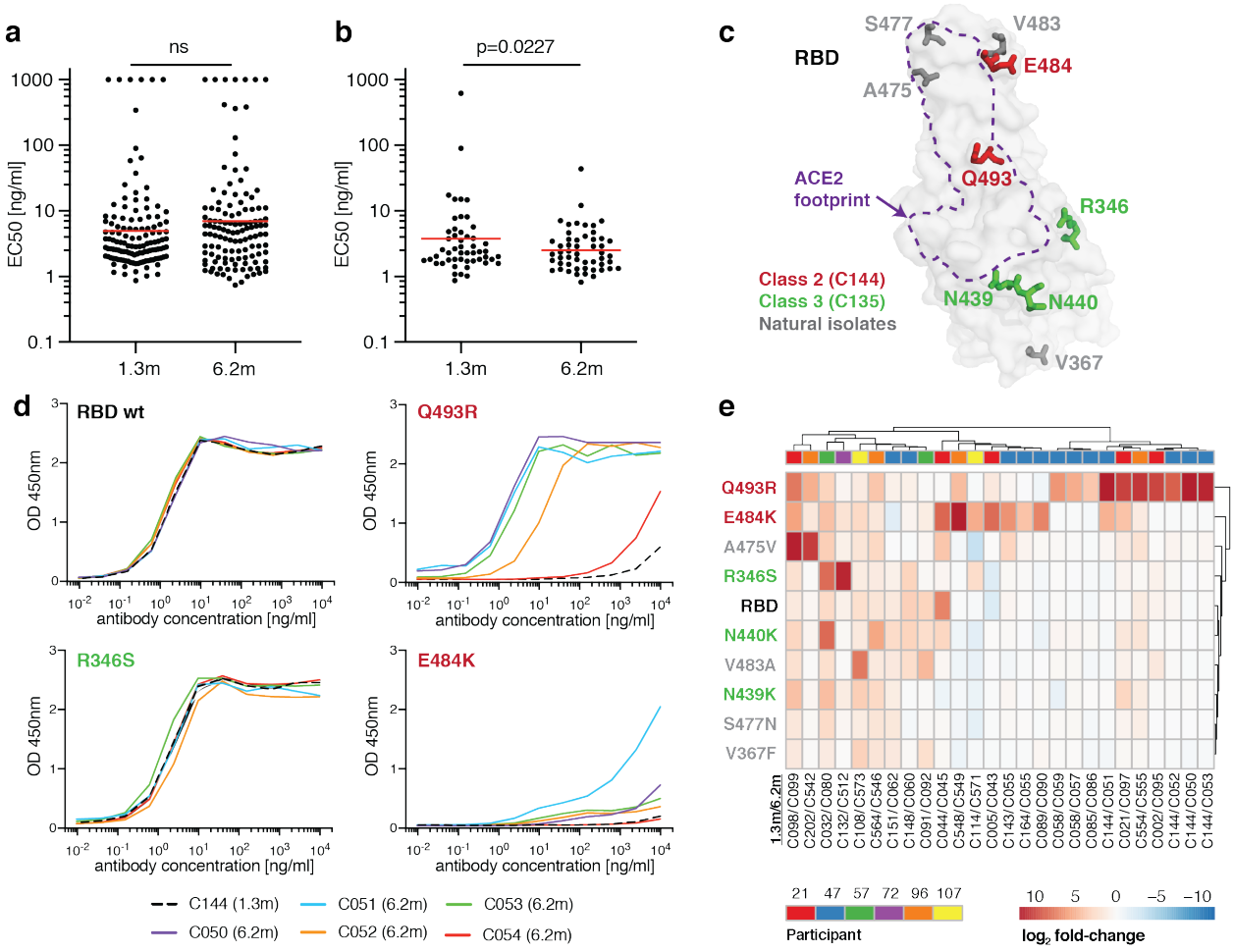

Fig. 3: Anti-SARS-CoV-2 RBD monoclonal antibody reactivity.

a, Graphs show anti-SARS-CoV-2 RBD antibody reactivity. ELISA EC_{50} values for all antibodies measured at 1.3 [1] and 122 selected monoclonal antibodies at 6.2 months. Horizontal bars indicate geometric mean. Statistical significance was determined using Mann–Whitney U-test. **b**, EC_{50} values for all antibodies that appear at 1.3 and 6.2 months. Average of two or more experiments. Horizontal bars indicate geometric mean. Statistical significance was determined using Wilcoxon matched-pairs signed rank test. **c,** Surface representation of the RBD with the ACE2 binding footprint indicated as a dotted line and selected residues found in circulating strains (grey) and residues that mediate resistance to class 2 (red, C144) and 3 (green, C135) antibodies highlighted

as sticks. **d.** Graphs show ELISA binding curves for C144 (black dashed line) and its clonal relatives obtained after 6.2 months (C050-54, solid lines) binding to wild type, Q493R, R346S, and E484K mutant RBDs. **e.** Heat map shows log2 relative fold change in EC_{50} against indicated RBD mutants for 26 antibody clonal pairs obtained at 1.3 and 6.2 month with the most pronounced changes in reactivity. The participant origin for each antibody pair is indicated above. All experiments were performed at least twice.

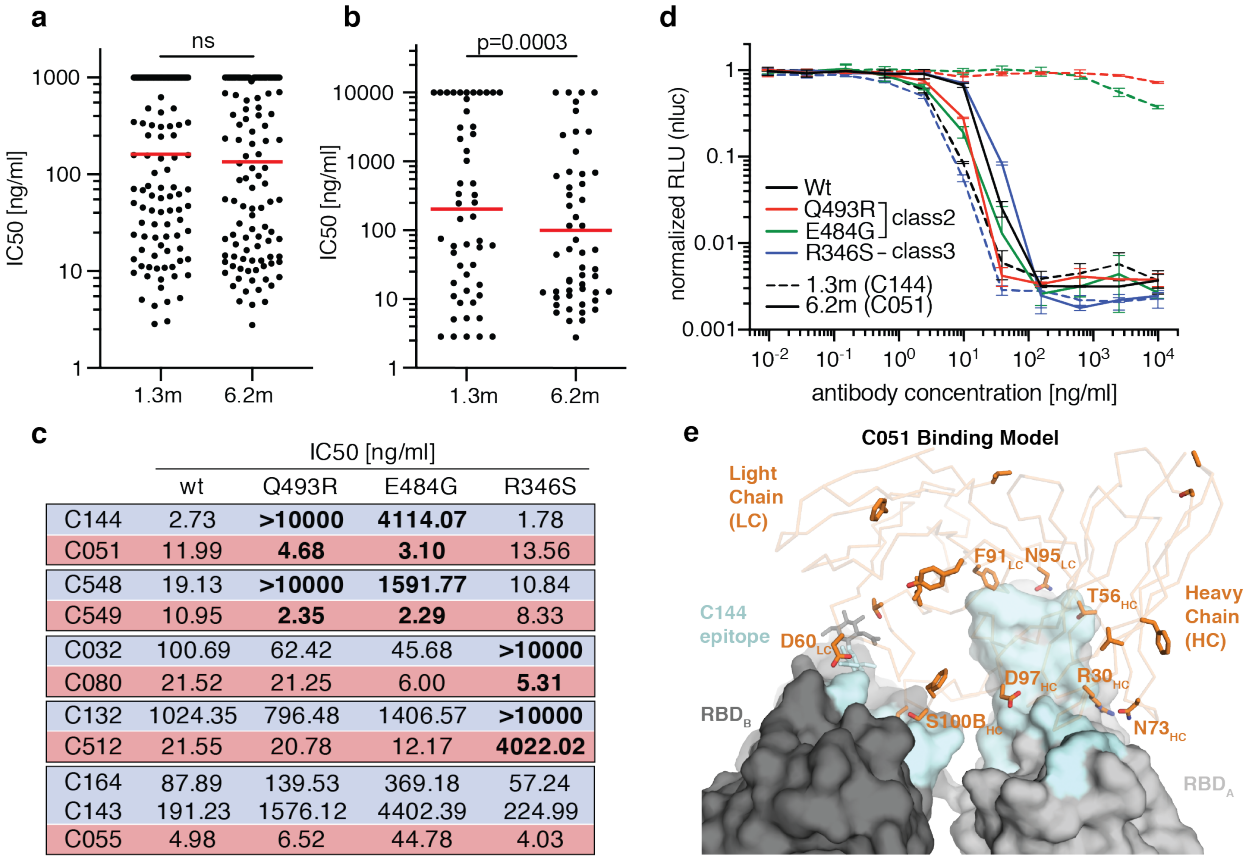

Fig.4: Anti-SARS-CoV-2 RBD monoclonal antibody neutralizing activity.

a, SARS-CoV-2 pseudovirus neutralization assay. IC_{50} values for all antibodies measured at 1.3 months[1] and 122 selected antibodies at 6.2 months. Antibodies with IC_{50} values above 1 µg/ml were plotted at 1 µg/ml. Mean of 2 independent experiments. Red bar indicates geometric mean.

294 Statistical significance was determined using Mann-Whitney U-test. **b,** IC50 values for antibodies
295 appearing at 1.3 and 6.2 months. Red bar indicates geometric mean. Statistical significance was
296 determined using Wilcoxon matched-pairs signed rank test. **c,** IC_{50} values for 5 different pairs of
297 mAb clonal relatives obtained after 1.3 (blue) or 6.2 months (red) for neutralization of wild type
298 and mutant SARS-CoV-2 pseudovirus. Antibody IDs of the 1.3 months/6.2 months mAb pairs as
299 indicated. **d,** Graph shows the normalized relative luminescence values for cell lysates of $293T_{ACE2}$
300 cells 48 hpi with SARS-CoV-2 pseudovirus harboring wt RBD or mutant RBDs (wt, Q493R,
301 E484G, R346S RBD mutants are shown in black, red, green and blue, respectively) in the presence
302 of increasing concentrations of mAbs C144 (1.3 months, dashed lines) or C051 (6.2 months, solid
303 lines). **e,** Surface representation of two adjacent "down" RBDs (RBD_A and RBD_B) on a spike
304 trimer with the C144 epitope on the RBDs highlighted in cyan and positions of amino acid
305 mutations that accumulated in C051 compared to the parent antibody C144 highlighted as stick
306 side chains on a Cα atom representation C051 V_HV_L binding to adjacent RBDs. The C051
307 interaction with two RBDs was modeled based on a cryo-EM structure of C144 Fab bound to spike
308 trimer [16].

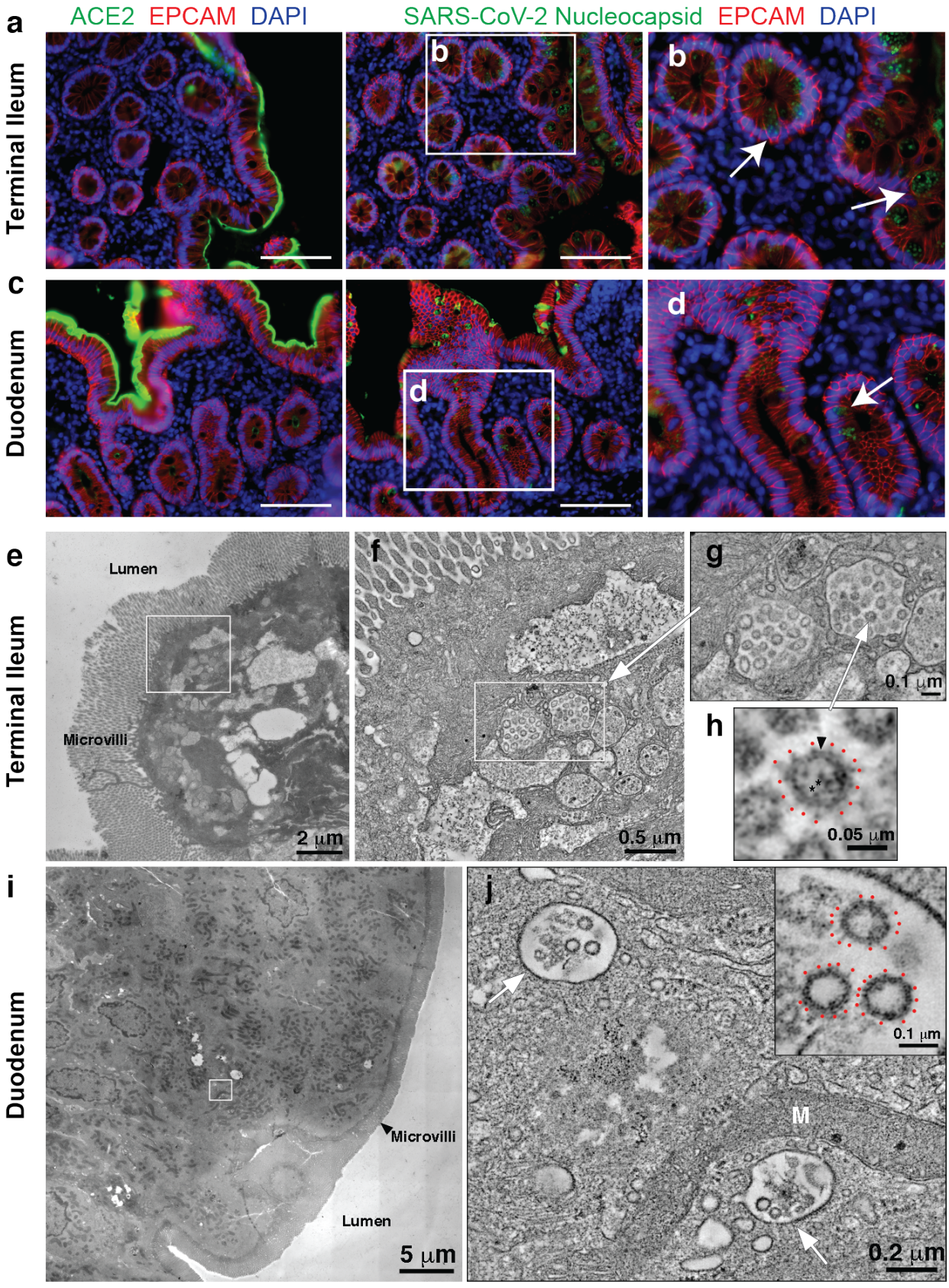

Fig. 5: Immunofluorescence and electron microscopy imaging of intestinal biopsies.

a, Immunofluorescence images of human enterocytes stained for EPCAM (red), DAPI (blue) and either ACE2 (green, **a** and **c**) or SARS-CoV-2 N (green, **b** and **d**) in intestinal biopsies taken 92 days after COVID-19 symptom onset of participant CGI-088 in the terminal ileum (**a-b**) or duodenum (**c-d**). Arrows indicate enterocytes with detectable SARS-CoV-2 antigen. White scale bar corresponds to 100 μm. **e-h**, SARS-CoV-2 virions within terminal ileum of CGI-088 (identified as described in methods). **e**, Montaged 2D overview of a region of apical epithelium. **f**, Tomographic slice (1.5 nm) of a 3D reconstruction of the area of epithelial cell cytoplasm indicated by the white square in **e**. Two coronavirus-filled exit compartments (center) are surrounded by other membranous compartments with dissimilar contents. **g**, Tomographic detail of the two exit compartments, indicated by the white rectangle in **f**. Each compartment contains ~20 presumptive SARS-CoV-2 virions. **h**, Detail of a single virion (indicated by white arrow in **g**) showing densities for the membrane bilayer (black arrowhead), punctate core structures (*), and surface spikes (red dots). **i-j,** SARS-CoV-2 within duodenum of CGI-088 (identified as described in methods). **i**, Montaged 2D overview of a region of the duodenal apical epithelium. **j**, Tomographic slice (1.5 nm) of a 3D reconstruction of the area of epithelial cell cytoplasm indicated by the white square in **i**. SARS-CoV-2 virions are localized to two smooth-walled exit compartments (white arrows). Inset in **j**: Detail of three presumptive SARS-CoV-2 virions from the compartment in the upper left of **j**. Surface spikes are indicated by red dots. M, Mitochondrion.

Methods

Data reporting

No statistical methods were used to predetermine sample size. The experiments were not randomized and the investigators were not blinded to allocation during experiments and outcome assessment.

Study participants. Previously enrolled study participants [1] were asked to return for a 6-month follow-up visit at the Rockefeller University Hospital in New York from August 31 through October 16, 2020. Eligible participants were adults aged 18-76 years and were either diagnosed with SARS-CoV-2 infection by RT-PCR (cases), or were close contacts (e.g., household, co-workers, members of same religious community) with someone who had been diagnosed with SARS-CoV-2 infection by RT-PCR (contacts). Close contacts without seroconversion against SARS-CoV-2 as assessed by serological assays (described below) were not included in the subsequent analysis. Most study participants were residents of the Greater New York City tri-state region and were asked to return approximately 6 months after the time of onset of COVID-19 symptoms. Participants presented to the Rockefeller University Hospital for blood sample collection and were asked to recall the symptoms and severity of clinical presentation during the acute (first 6 weeks) and the convalescent (7 weeks until second study visit) phase of COVID-19, respectively. The severity of acute infection was assessed by the WHO Ordinal Clinical Progression/Improvement Scale (https://www.who.int/publications/i/item/covid-19-therapeutic-trial-synopsis). Shortness of breath was assessed through the modified Medical Research Council (mMRC) dyspnea scale [39]. Participants who presented with persistent symptoms attributable to COVID-19 were identified on the basis of chronic shortness of breath or fatigue, deficit in athletic

ability and/or three or more additional long-term symptoms such as persistent unexplained fevers, chest pain, new-onset cardiac sequalae, arthralgias, impairment of concentration/mental acuity, impairment of sense of smell/taste, neuropathy or cutaneous findings [2,3]. All participants at Rockefeller University provided written informed consent before participation in the study and the study was conducted in accordance with Good Clinical Practice.

Gastrointestinal biopsy cohort. To determine if SARS-CoV-2 can persist in the gastrointestinal tract, we recruited a cohort of 14 individuals with prior diagnosis of and recovery from COVID-19 illness. Eligible participants included adults, 18-76 years of age who were previously diagnosed with SARS-CoV-2 by RT PCR and presented to the gastroenterology clinics of Mount Sinai Hospital. Endoscopic procedures were performed for clinically indicated conditions as detailed in Supplementary Table 7. All participants were asymptomatic at the time of the endoscopic procedures and negative for SARS-CoV-2 by nasal swab PCR (Cycle threshold (Ct) cut-off <38[40]). Informed consent was obtained from all participants. The biopsy-related studies were approved by the Mount Sinai Ethics Committee/IRB (IRB 16-0583, The impact of viral infections and their treatment on gastrointestinal immune cells).

SARS-CoV-2 saliva PCR test

Saliva was collected into guanidine thiocyanate buffer as described [41]. RNA was extracted using either a column-based (Qiagen QIAmp DSP Viral RNA Mini Kit, Cat#61904) or a magnetic bead-based method as described [42]. Reverse transcribed cDNA was amplified using primers and probes validated by the CDC or by Columbia University Personalized Medicine Genomics Laboratory,

respectively, and approved by the FDA under the Emergency Use Authorization. Viral RNA was considered detected if the cycle threshold (Ct) for two viral primers/probes were <40.

Blood samples processing and storage. Peripheral Blood Mononuclear Cells (PBMCs) were obtained by gradient centrifugation and stored in liquid nitrogen in the presence of FCS and DMSO. Heparinized plasma and serum samples were aliquoted and stored at -20°C or less. Prior to experiments, aliquots of plasma samples were heat-inactivated (56°C for 1 hour) and then stored at 4°C.

High throughput automated serology assays

Plasma samples from 80 out of 87 participants were tested by high throughput automated serology assays. The Roche Elecsys anti-SARS-CoV-2 assay was performed on Roche Cobas e411 (Roche Diagnostics, Indianapolis, IN). The Elecsys anti-SARS-CoV-2 assay uses a recombinant protein representing the N antigen for the determination of antibodies against SARS-CoV-2. This assay received Emergency Use Authorization (EUA) approval from the United States Food and Drug Administration (FDA) [5]. The Pylon COVID-19 IgG and IgM assays were used to measure plasma IgG and IgM antibodies against SARS-CoV-2, respectively. Plasma samples were assayed on the Pylon 3D analyzer (ET HealthCare, Palo Alto, CA) as previously described [4]. This assay was implemented clinically as a laboratory-developed test under New York State Department of Health regulations. Briefly, the assay was performed using a unitized test strip containing wells with pre-dispensed reagents. The COVID-19 reagent contains biotinylated recombinant versions of the SARS-CoV-2 S-Protein RBD and trace amounts of N protein as antigens that bind IgG and IgM, respectively. The cut off values for both Pylon assays were determined using the mean of non-

399 COVID-19 samples plus 6 Standard Deviations (SDs). The results of a sample are reported in the
400 form of a cutoff index (COI) or an index value (IV), which were determined by the instrument
401 readout of the test sample divided by instrument readout at cut off.
402
403 **ELISAs**
404 Validated ELISAs [43,44] to evaluate antibodies binding to SARS-CoV-2 RBD and additional RBDs
405 were performed by coating of high-binding 96-half-well plates (Corning 3690) with 50 µl per well
406 of a 1µg/ml protein solution in PBS overnight at 4 °C. Plates were washed 6 times with washing
407 buffer (1× PBS with 0.05% Tween-20 (Sigma-Aldrich)) and incubated with 170 µl per well
408 blocking buffer (1× PBS with 2% BSA and 0.05% Tween-20 (Sigma)) for 1 h at room temperature.
409 Immediately after blocking, monoclonal antibodies or plasma samples were added in PBS and
410 incubated for 1 h at room temperature. Plasma samples were assayed at a 1:67 starting dilution and
411 7 additional threefold serial dilutions. Monoclonal antibodies were tested at 10 µg/ml starting
412 concentration and 10 additional fourfold serial dilutions. Plates were washed 6 times with washing
413 buffer and then incubated with anti-human IgG, IgM or IgA secondary antibody conjugated to
414 horseradish peroxidase (HRP) (Jackson Immuno Research 109-036-088 109-035-129 and Sigma
415 A0295) in blocking buffer at a 1:5,000 dilution (IgM and IgG) or 1:3,000 dilution (IgA). Plates
416 were developed by addition of the HRP substrate, TMB (ThermoFisher) for 10 min (plasma
417 samples) or 4 minutes (monoclonal antibodies), then the developing reaction was stopped by
418 adding 50 µl 1 M H_2SO_4 and absorbance was measured at 450 nm with an ELISA microplate
419 reader (FluoStar Omega, BMG Labtech) with Omega and Omega MARS software for analysis.
420 For plasma samples, a positive control (plasma from patient COV72, diluted 66.6-fold and seven
421 additional threefold serial dilutions in PBS) was added to every assay plate for validation. The

422 average of its signal was used for normalization of all of the other values on the same plate with
423 Excel software before calculating the area under the curve using Prism V8.4 (GraphPad). For
424 monoclonal antibodies, the EC50 was determined using four-parameter nonlinear regression
425 (GraphPad Prism V8.4).
426
427 **Expression of RBD proteins**
428 Mammalian expression vectors encoding the RBDs of SARS-CoV-2 (GenBank MN985325.1; S
429 protein residues 319-539) and eight additional mutant RBD proteins (E484K, Q493R, R346S,
430 N493K, N440K, V367F, A475V, S477N and V483A) with an N-terminal human IL-2 or Mu
431 phosphatase signal peptide were previously described [45].
432
433 **SARS-CoV-2 pseudotyped reporter virus**
434 SARS-CoV-2 pseudotyped particles were generated as previously described [1,46]. Briefly, 293T
435 cells were transfected with pNL4-3ΔEnv-nanoluc and pSARS-CoV-2-$S_{\Delta 19}$. For generation of
436 RBD-mutant pseudoviruses, pSARS-CoV-2-$S_{\Delta 19}$ carrying either of the following spike mutations
437 was used instead of its wt counterpart: Q493R, R346S or E484G [47]. Particles were harvested 48
438 hpt, filtered and stored at -80°C.
439
440 **Pseudotyped virus neutralization assay**
441 Fourfold serially diluted plasma from COVID-19-convalescent individuals or monoclonal
442 antibodies were incubated with SARS-CoV-2 pseudotyped virus for 1 h at 37 °C. The mixture was
443 subsequently incubated with $293T_{Ace2}$ cells for 48 h after which cells were washed with PBS and
444 lysed with Luciferase Cell Culture Lysis 5× reagent (Promega). Nanoluc Luciferase activity in

lysates was measured using the Nano-Glo Luciferase Assay System (Promega) with the Glomax Navigator (Promega). The obtained relative luminescence units were normalized to those derived from cells infected with SARS-CoV-2 pseudotyped virus in the absence of plasma or monoclonal antibodies. The half-maximal inhibitory concentration for plasma (NT_{50}) or monoclonal antibodies (IC_{50}) was determined using four-parameter nonlinear regression (least squares regression method without weighting; constraints: top=1, bottom=0) (GraphPad Prism).

Biotinylation of viral protein for use in flow cytometry

Purified and Avi-tagged SARS-CoV-2 RBD was biotinylated using the Biotin-Protein Ligase-BIRA kit according to manufacturer's instructions (Avidity) as described before [1]. Ovalbumin (Sigma, A5503-1G) was biotinylated using the EZ-Link Sulfo-NHS-LC-Biotinylation kit according to the manufacturer's instructions (Thermo Scientific). Biotinylated ovalbumin was conjugated to streptavidin-BV711 (BD biosciences, 563262) and RBD to streptavidin-PE (BD Biosciences, 554061) and streptavidin-AF647 (Biolegend, 405237)[1].

Single-cell sorting by flow cytometry

Single-cell sorting by flow cytometry was described previously [1]. Briefly, peripheral blood mononuclear cells were enriched for B cells by negative selection using a pan-B-cell isolation kit according to the manufacturer's instructions (Miltenyi Biotec, 130-101-638). The enriched B cells were incubated in FACS buffer (1× PBS, 2% FCS, 1 mM EDTA) with the following anti-human antibodies (all at 1:200 dilution): anti-CD20-PECy7 (BD Biosciences, 335793), anti-CD3-APC-eFluro 780 (Invitrogen, 47-0037-41), anti-CD8-APC-eFluor 780 (Invitrogen, 47-0086-42), anti-CD16-APC-eFluor 780 (Invitrogen, 47-0168-41), anti-CD14-APC-eFluor 780 (Invitrogen, 47-

468 0149-42), as well as Zombie NIR (BioLegend, 423105) and fluorophore-labelled RBD and
469 ovalbumin (Ova) for 30 min on ice. Single CD3−CD8−CD14−CD16−CD20+Ova−RBD-
470 PE+RBD-AF647+ B cells were sorted into individual wells of 96-well plates containing 4 µl of
471 lysis buffer (0.5× PBS, 10 mM DTT, 3,000 units/ml RNasin Ribonuclease Inhibitors (Promega,
472 N2615) per well using a FACS Aria III and FACSDiva software (Becton Dickinson) for
473 acquisition and FlowJo for analysis. The sorted cells were frozen on dry ice, and then stored at
474 −80 °C or immediately used for subsequent RNA reverse transcription.
475
476 **Antibody sequencing, cloning and expression**
477 Antibodies were identified and sequenced as described previously [1]. In brief, RNA from single
478 cells was reverse-transcribed (SuperScript III Reverse Transcriptase, Invitrogen, 18080-044) and
479 the cDNA stored at −20 °C or used for subsequent amplification of the variable IGH, IGL and IGK
480 genes by nested PCR and Sanger sequencing. Sequence analysis was performed using MacVector.
481 Amplicons from the first PCR reaction were used as templates for sequence- and ligation-
482 independent cloning into antibody expression vectors. Recombinant monoclonal antibodies and
483 Fabs were produced and purified as previously described [1].
484
485 **Computational analyses of antibody sequences**
486 Antibody sequences were trimmed based on quality and annotated using Igblastn v.1.14. with
487 IMGT domain delineation system. Annotation was performed systematically using Change-O
488 toolkit v.0.4.540 [48]. Heavy and light chains derived from the same cell were paired, and clonotypes
489 were assigned based on their V and J genes using in-house R and Perl scripts (Extended data Fig.4).

All scripts and the data used to process antibody sequences are publicly available on GitHub (https://github.com/stratust/igpipeline).

The frequency distributions of human V genes in anti-SARS-CoV-2 antibodies from this study was compared to 131,284,220 IgH and IgL sequences generated by [49] and downloaded from cAb-Rep[50], a database of human shared BCR clonotypes available at https://cab-rep.c2b2.columbia.edu/. Based on the 82 distinct V genes that make up the 1703 analyzed sequences from Ig repertoire of the three patients present in this study, we selected the IgH and IgL sequences from the database that are partially coded by the same V genes and counted them according to the constant region. The frequencies shown in (Fig. S4**)** are relative to the source and isotype analyzed. We used the two-sided binomial test to check whether the number of sequences belonging to a specific IgHV or IgLV gene in the repertoire is different according to the frequency of the same IgV gene in the database. Adjusted p-values were calculated using the false discovery rate (FDR) correction. Significant differences are denoted with stars.

Nucleotide somatic hypermutation and CDR3 length were determined using in-house R and Perl scripts. For somatic hypermutations, IGHV and IGLV nucleotide sequences were aligned against their closest germlines using Igblastn and the number of differences were considered nucleotide mutations. The average mutations for V genes was calculated by dividing the sum of all nucleotide mutations across all patients by the number of sequences used for the analysis. To calculate the GRAVY scores of hydrophobicity [51] we used Guy H.R. Hydrophobicity scale based on free energy of transfer (kcal/mole) [52] implemented by the R package Peptides (the Comprehensive R Archive Network repository; https://journal.r-project.org/archive/2015/RJ-2015-001/RJ-2015-001.pdf).

We used 532 heavy chain CDR3 amino acid sequences from this study and 22,654,256 IGH CDR3 sequences from the public database of memory B cell receptor sequences [53]. The Shapiro–Wilk test was used to determine whether the GRAVY scores are normally distributed. The GRAVY scores from all 532 IGH CDR3 amino acid sequences from this study were used to perform the test and 5,000 GRAVY scores of the sequences from the public database were randomly selected. The Shapiro–Wilk P values were 6.896 × 10−3 and 2.217 × 10−6 for sequences from this study and the public database, respectively, indicating that the data were not normally distributed. Therefore, we used the Wilcoxon nonparametric test to compare the samples, which indicated a difference in hydrophobicity distribution (P = 5 × 10−6) (Extended data Fig.7).

Heatmap of log2 relative fold change in EC50 against the indicated RBD mutants for antibody clonal pairs obtained at 1.3 and 6.2 months (Fig.3e and Extended data Fig. 8k) was created with R pheatmap package (https://github.com/raivokolde/pheatmap) using Euclidean distance and Ward.2 clustering method.

Biopsies and Immunofluorescence

Endoscopically obtained mucosal biopsies were formalin fixed and paraffin embedded. Sections (5µm) were cut, dewaxed in xylene, and rehydrated in graded alcohol and phosphate-buffered saline (PBS). Heat-induced epitope retrieval was performed in target retrieval solution (Dako, S1699) using a commercial pressure cooker. Slides were then cooled to room temperature, washed in PBS and permeabilized for 30 minutes in 0.1% tritonX-100 in PBS. Non-specific binding was blocked with 10% goat serum (Invitrogen, 50062Z) for 1 hour at room temperature. Sections were then incubated with a combination of primary antibodies diluted in blocking solution overnight at

536 4°C. Slides were washed 3 times in PBS and then incubated in secondary antibody and 4′,6-
537 diamidino-2-phenylindole (1ug/mL) for 1 hour at room temperature. Sections were washed in PBS
538 3 times and then mounted with Fluoromount-G (Electron Microscopy Sciences, 1798425).
539 Controls included, omitting primary antibody (no primary 995 control), or substituting primary
540 antibodies with non-reactive antibodies of the same isotype (isotype control). A Nikon Eclipse Ni
541 microscope and digital SLR camera (Nikon, DS-Qi2) was used to visualize and image the tissue.
542
543 The antibody used to stain sections for N protein was raised in rabbits against SARS-CoV N and
544 is cross-reactive with SARS-CoV-2 N protein [54].
545

Antigen	Clone	Vendor	Catalogue number	Host species	Conjugate	Dilution
ACE2	Polyclonal	Abcam	ab15348	rabbit	unconjugated	1:1000
EPCAM	SPM491	GeneTex	GTX34693	mouse	unconjugated	1:100
SARS-CoV-2 nucleocapsid	Polyclonal	Spiegel, M. *et al.* [54]	N/A	rabbit	unconjugated	1:2000
No known specificity (isotype control)	Polyclonal	Abcam	ab37415	rabbit	unconjugated	variable
Yeast GAL4 (isotype control)	15-6E10A7	Abcam	ab170190	mouse	unconjugated	variable
Mouse IgG H&L	Polyclonal	Abcam	ab150116	goat	Alexa Fluor 594	1:1000

Rabbit IgG H&L	Polyclonal	Abcam	ab150077	goat	Alexa Fluor 488	1:1000

SARS-CoV-2 PCR (intestinal biopsies)

To determine if SARS-CoV-2 RNA is present in the gastrointestinal tract we isolated RNA from endoscopically obtained mucosal biopsies using Direct-zol miniprep kit (Zymo research, Cat. No. R2050). Reverse transcribed cDNA was amplified using 2019-nCov Ruo Kit (IDT) to detect viral nucleocapsid genomic RNA. Amplification of sub-genomic nucleocapsid RNA was done using following primers and probe: sgLeadSARSCov2_F 5'-CGATCTCTTGTAGATCTGTTCTC -3'[26], wtN_R4 5' – GGTGAACCAAGACGCAGTAT – 3', wtN_P4 5' – /56-FAM/TAACCAGAA/ZEN/TGGAGAACGCAGTGGG/3IABkFQ/ – 3'. Quantitative PCR was performed using QuantTect probe PCR kit (Qiagen, Cat. No. 204345) under following conditions: 95 15', 95°C 15 sec, 60°C 1 min using the Applied Biosystem QuantStudio 6 Flex Real-Time PCR System. Viral RNA was considered detected if the cycle threshold (Ct) for viral primers/probes was <40. Samples from positive wells were column purified and presence of N1 sequences additionally verified by Sanger sequencing.

Electron Microscopy and Dual-Axis Tomography

Tissues samples were fixed with 3% glutaraldehyde to meet biosafety requirements. Tissues were rinsed with cold 0.1M sodium cacodylate trihydrate + 5% sucrose and further dissected to block sizes sufficient for embedding and sectioning. Tissues were postfixed for 1 h with cold 2% osmium tetroxide in cacodylate buffer, en bloc stained with 1% aqueous uranyl acetate, dehydrated with acetone and embedded in Epon-Araldite resin (Electron Microscopy Sciences). Samples were flat-embedded between two Teflon-coated glass microscope slides and the resin polymerized at 60 °C

568 for 24 h. Embedded tissue blocks were observed by light microscopy to ascertain preservation
569 quality and select regions of interest (i.e., apical epithelium). Blocks were extracted with a scalpel
570 and glued to plastic sectioning stubs prior to sectioning. Semi-thin (150 nm) serial sections were
571 cut with a UC6 ultramicrotome (Leica Microsystems) using a diamond knife (Diatome, Ltd.
572 Switzerland). Sections were placed on formvar-coated copper-rhodium slot grids (Electron
573 Microscopy Sciences) and stained with 3% uranyl acetate and lead citrate. Colloidal gold particles
574 (10 nm) were placed on both surfaces of the grids to serve as fiducial markers for tomographic
575 image alignment. Grids were placed in a dual-axis tomography holder (Model 2010, E.A.
576 Fischione Instruments, Export PA) and imaged with a Tecnai G2 T12 transmission electron
577 microscope (120 KeV; ThermoFisher Scientific). Images were recorded with a 2k x 2k CCD
578 camera (XP1000; Gatan, Pleasonton, CA). Tomographic tilt series and large-area montages were
579 acquired automatically using the SerialEM software package [55]. For dual-axis tomography, images
580 were collected at 1° intervals as samples were tilted +/- 62°. The grid was then rotated 90° and a
581 second tilt-series was acquired about the orthogonal axis. Tomograms were calculated, analyzed
582 and modeled using the IMOD software package [56,57] on MacPro and iMac Pro computers (Apple,
583 Inc).
584
585 Presumptive SARS-CoV-2 virions were identified from tomographic reconstructions of tissue
586 samples by observing structures resembling virions described in cryo-electron tomography studies
587 of purified SARS-CoV-2 and SARS-CoV-2 in infected cells [58-61]. We used the following criteria
588 for SARS-CoV-2 virion identification in tissues: (*i*) Structures that were spherical in 3D and not
589 continuous with other adjacent structures with ~60-120 nM diameters, (*ii*) Spherical structures
590 with densities corresponding to a distinct membrane bilayer, internal puncta consistent with

591 ribonucleoproteins [58], and densities corresponding to surface spikes on the external peripheries of
592 the spheres.
593
594 **Competing interests:** The Rockefeller University has filed a provisional patent application in
595 connection with this work on which D.F.R. and M.C.N. are inventors (US patent 63/021,387).
596
597 **Data availability statement:** Data are provided in SI Tables 1-7. The raw sequencing data
598 associated with Figure 2 has been deposited at Github (https://github.com/stratust/igpipeline). This
599 study also uses data from "A Public Database of Memory and Naive B-Cell Receptor Sequences"
600 (https://doi.org/10.5061/dryad.35ks2), PDB (6VYB and 6NB6) and from "High frequency of
601 shared clonotypes in human B cell receptor repertoires" (https://doi.org/10.1038/s41586-019-
602 0934-8)
603
604 **Code availability statement:** Computer code to process the antibody sequences is available at
605 GitHub (https://github.com/stratust/igpipeline).
606
607 **Acknowledgements:** We thank all study participants who devoted time to our research; Drs. Barry
608 Coller and Sarah Schlesinger, the Rockefeller University Hospital Clinical Research Support
609 Office and nursing staff. Mayu Okawa Frank and Robert B. Darnell for SARS-CoV-2 saliva PCR
610 testing. Charles M. Rice and all members of the M.C.N. laboratory for helpful discussions and
611 Maša Jankovic for laboratory support. This work was supported by NIH grant P01-AI138398-S1
612 (M.C.N. and P.J.B.) and 2U19AI111825 (M.C.N.).; the Caltech Merkin Institute for Translational
613 Research and P50 AI150464-13 (P.J.B.), George Mason University Fast Grant (D.F.R. and P.J.B.)

614 and the European ATAC consortium EC 101003650 (D.F.R.); R37-AI64003 to P.D.B.;
615 R01AI78788 to T.H.; We thank Dr. Jost Vielmetter and the Protein Expression Center in the
616 Beckman Institute at Caltech for expression assistance. Electron microscopy was performed in the
617 Caltech Beckman Institute Resource Center for Transmission Electron Microscopy. C.O.B. is
618 supported by the HHMI Hanna Gray and Burroughs Wellcome PDEP fellowships. C.G. was
619 supported by the Robert S. Wennett Post-Doctoral Fellowship, in part by the National Center for
620 Advancing Translational Sciences (National Institutes of Health Clinical and Translational Science
621 Award program, grant UL1 TR001866), and by the Shapiro-Silverberg Fund for the Advancement
622 of Translational Research. P.D.B. and M.C.N. are Howard Hughes Medical Institute Investigators.
623

624 **Author Contributions:** C.G., P.D.B., P.J.B., T.H., S.B. and M.C.N. conceived, designed and
625 analyzed the experiments. D.F.R., M.Caskey. and C.G. designed clinical protocols. Z.W., J.C.C.L.,
626 F.M., S.F., M.T., M.L., A.C., M.J., D.S.B., F.S., Y.W., C.V., C.O.B., K.G., D.J., J.Y. and Z.Z.
627 carried out experiments. A.G. and M.Cipolla produced antibodies. A.H., D.S.B., M.Turroja,
628 K.G.M., M.Tankelevich, C.G. and M.Caskey recruited participants and executed clinical
629 protocols. I.S. processed clinical samples. T.Y.O. performed bioinformatic analysis. C.G, P.D.B.,
630 P.J.B., T.H., S.B. and M.C.N. wrote the manuscript with input from all co-authors.
631

Extended Data Figures

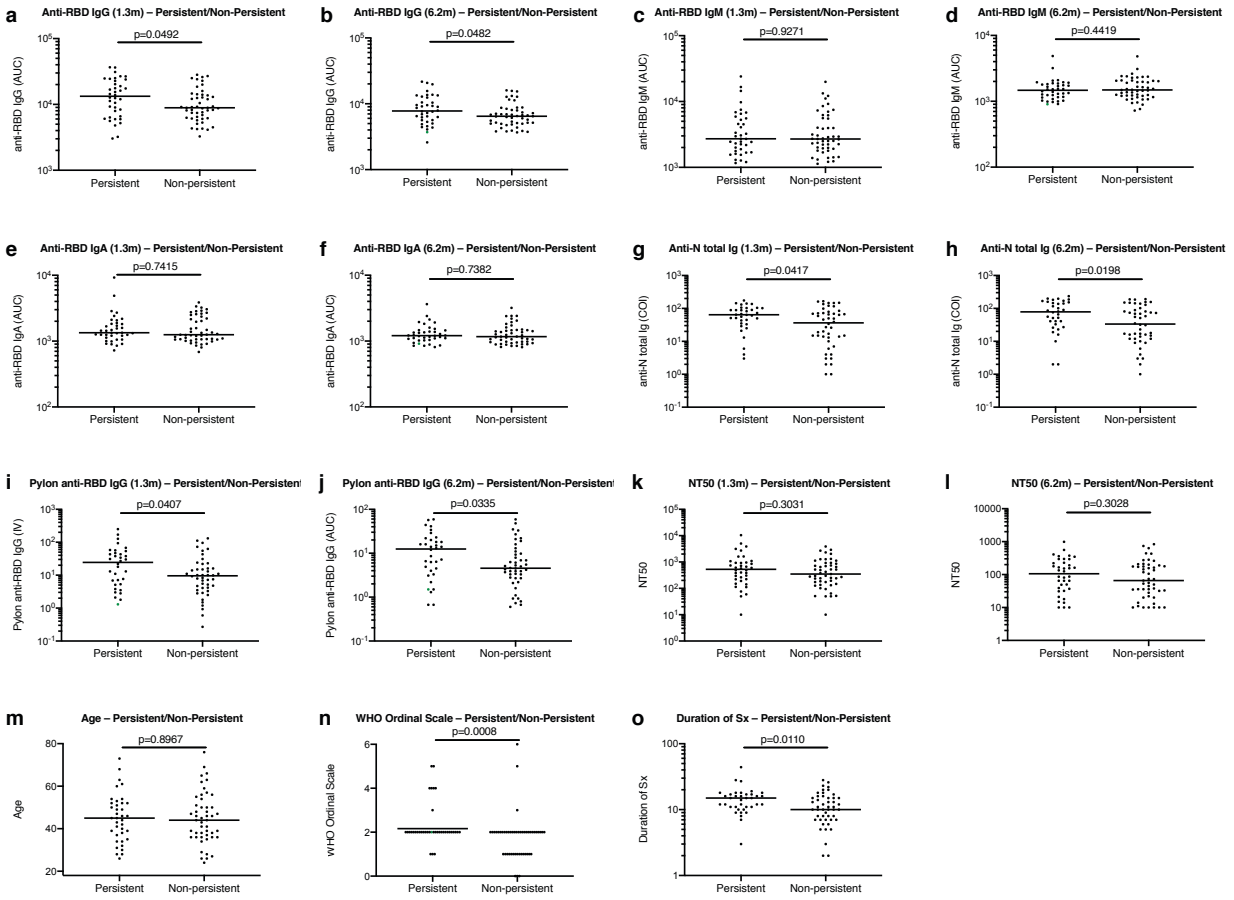

Extended Data Fig. 1: Clinical correlates of plasma antibody titres. **a**, Normalized AUC anti-RBD IgG titres at 1.3 months for participants with (n=38) or without (n=49) persistent post-acute symptoms. **b**, Normalized AUC anti-RBD IgG titres at 6.2 months for participants with (n=38) or without (n=49) persistent post-acute symptoms. **c**, Normalized AUC anti-RBD IgM titres at 1.3 months for participants with (n=38) or without (n=49) persistent post-acute symptoms. **d**, Normalized AUC anti-RBD IgM titres at 6.2 months for participants with (n=38) or without (n=49) persistent post-acute symptoms. **e**, Normalized AUC anti-RBD IgA titres at 1.3 months for participants with (n=38) or without (n=49) persistent post-acute symptoms. **f**, Normalized AUC anti-RBD IgA titres at 6.2 months for participants with (n=38) or without (n=49)

643 persistent post-acute symptoms. **g**, COI values of anti-N total Ig titres at 1.3 months for participants
644 with (n=38) or without (n=49) persistent post-acute symptoms. **h**, COI values of anti-N total Ig
645 titres at 6.2 months for participants with (n=38) or without (n=49) persistent post-acute symptoms.
646 **i**, IV values of anti-RBD IgG titres at 1.3 months for participants with (n=38) or without (n=49)
647 persistent post-acute symptoms. **j**, IV values of anti-RBD IgG titres at 6.2 months for participants
648 with (n=38) or without (n=49) persistent post-acute symptoms. **k**, NT50 values at 1.3 months for
649 participants with (n=38) or without (n=49) persistent post-acute symptoms. **l**, NT50 values at 6.2
650 months for participants with (n=38) or without (n=49) persistent post-acute symptoms. **m**, Age in
651 years for participants with (n=38) or without (n=49) persistent post-acute symptoms. **n**, Severity
652 of acute infection as assessed by the WHO Ordinal Clinical Progression/Improvement Scale for
653 participants with (n=38) or without (n=49) persistent post-acute symptoms. **o**, Duration of
654 Symptoms during acute infection for participants with (n=38) or without (n=49) persistent post-
655 acute symptoms. Horizontal bars indicate median values. Statistical significance was determined
656 using Mann–Whitney U-tests.

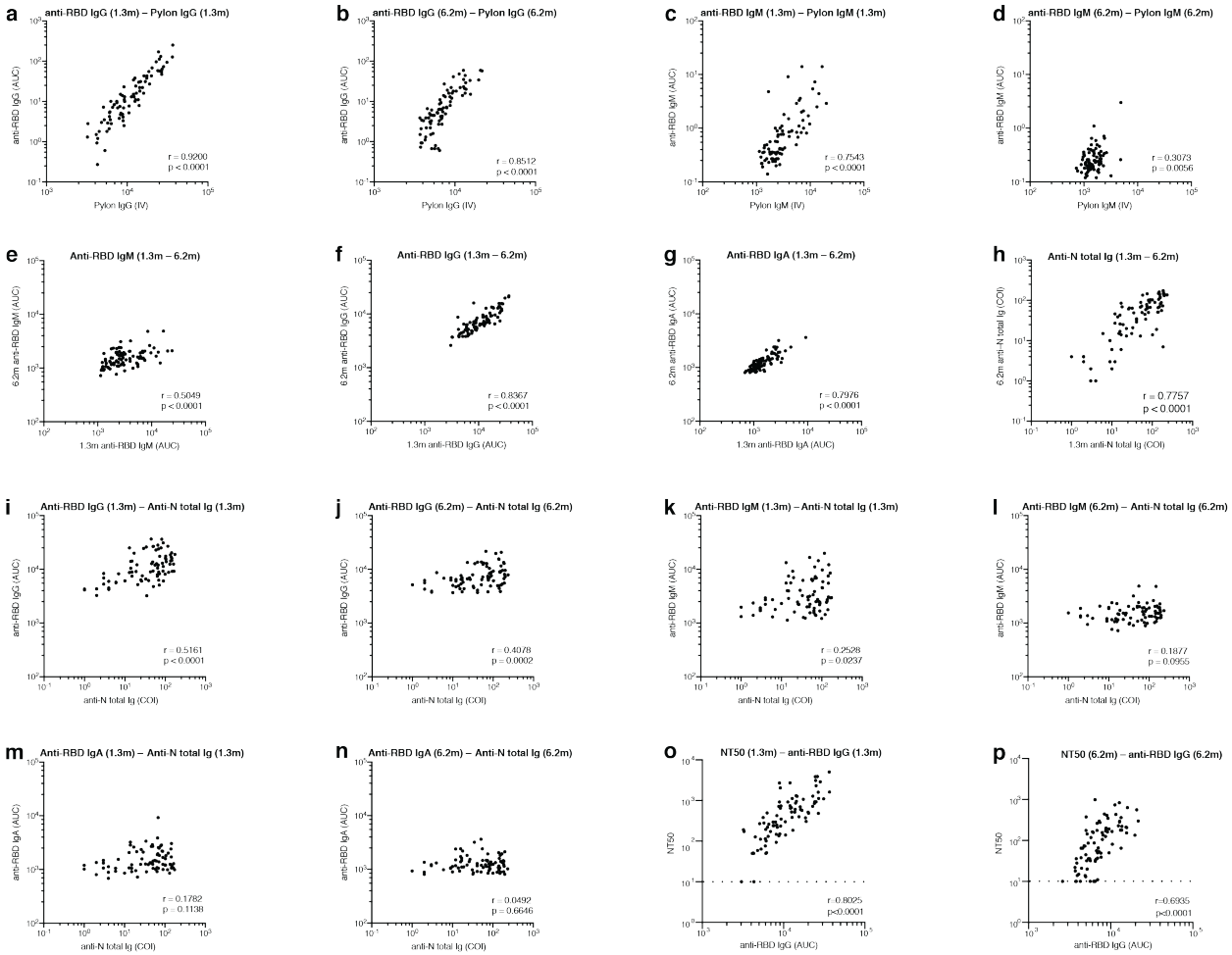

Extended Data Fig. 2: Correlations of plasma antibody measurements.

a, Normalized AUC for IgG anti-RBD plotted against Pylon IgG anti-RBD index values at 1.3 months. **b,** Normalized AUC for IgG anti-RBD plotted against Pylon IgG anti-RBD index values at 6.2 months. **c,** Normalized AUC for IgM anti-RBD plotted against Pylon IgM anti-RBD index values at 1.3 months. **d,** Normalized AUC for IgM anti-RBD plotted against Pylon IgM anti-RBD index values at 6.2 months. **e**, Normalized AUC for IgM anti-RBD at 6.2 months plotted against IgM anti-RBD at 1.3 months. **f**, Normalized AUC for IgG anti-RBD at 6.2 months plotted against IgG anti-RBD at 1.3 months. **g**, Normalized AUC for IgA anti-RBD at 6.2 months plotted against IgA anti-RBD at 1.3 months. **h**, COI values for anti-N total Ig titres at 6.2 months plotted against

667 anti-N total Ig titres at 1.3 months. **i**, Anti-RBD IgG titres at 1.3 months plotted against anti-N total
668 Ig titres at 1.3 months. **j**, Anti-RBD IgG titres at 6.2 months plotted against anti-N total Ig titres at
669 6.2 months. **k,** Anti-RBD IgM titres at 1.3 months plotted against anti-N total Ig titres at 1.3
670 months. **l**, Anti-RBD IgM titres at 6.2 months plotted against anti-N total Ig titres at 6.2 months.
671 **m,** Anti-RBD IgA titres at 1.3 months plotted against anti-N total Ig titres at 1.3 months. **l**, Anti-
672 RBD IgA titres at 6.2 months plotted against anti-N total Ig titres at 6.2 months. **o**, NT50 values at
673 1.3 months plotted against anti-RBD IgG titres at 1.3 months. **p**, NT50 values at 6.2 months plotted
674 against anti-RBD IgG titres at 6.2 months. The *r* and *p* values were determined by two-tailed
675 Spearman's correlations.

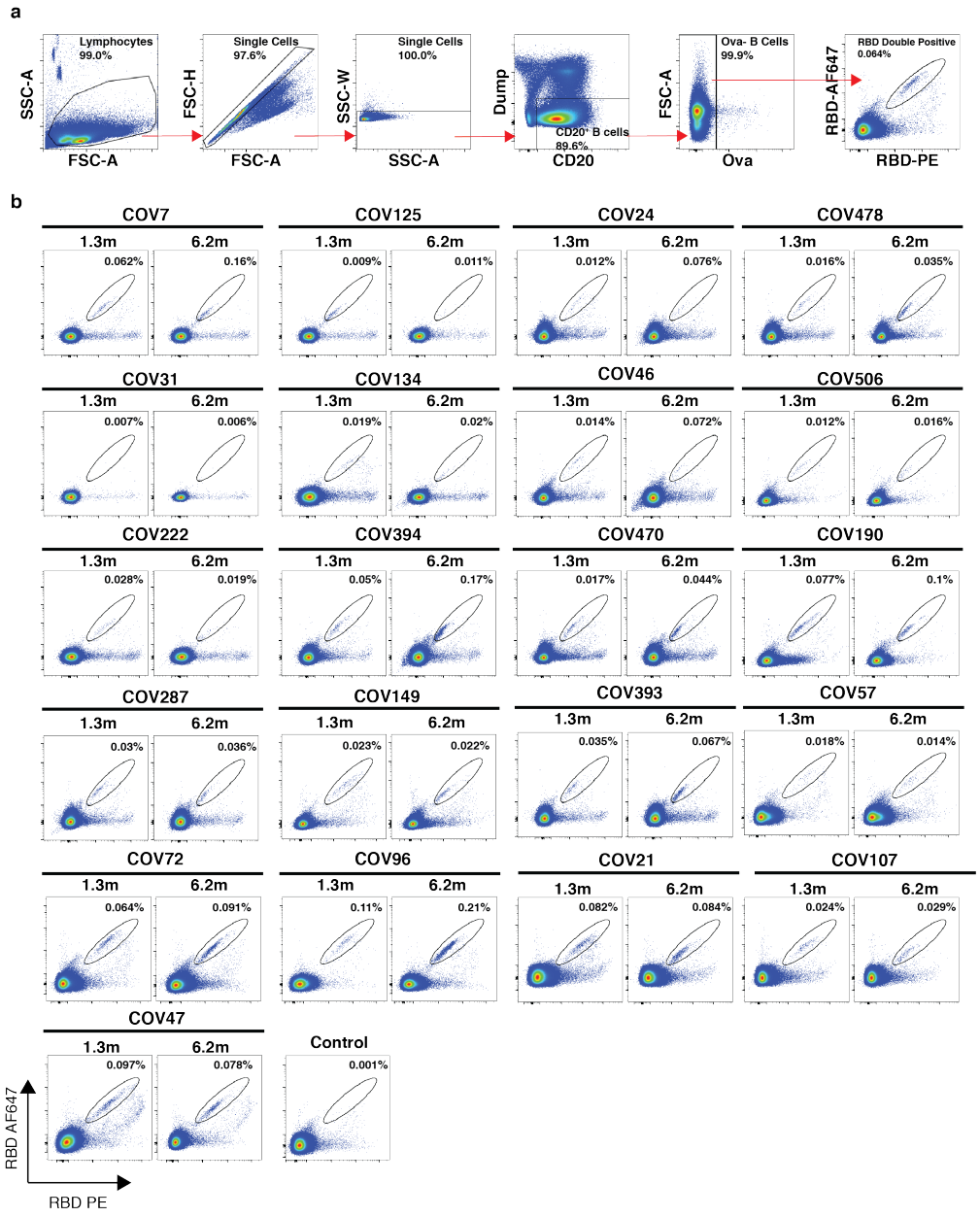

676

677 **Extended Data Fig. 3: Flow cytometry.**

678 **a,** Gating strategy used for cell sorting. Gating was on singlets that were CD20+ and
679 CD3−CD8−CD16−Ova−. Sorted cells were RBD-PE+ and RBD-AF647+. **b,** Flow cytometry
680 showing the percentage of RBD-double positive memory B cells from month 1.3 or month 6 post-
681 infection in 21 randomly selected patients.

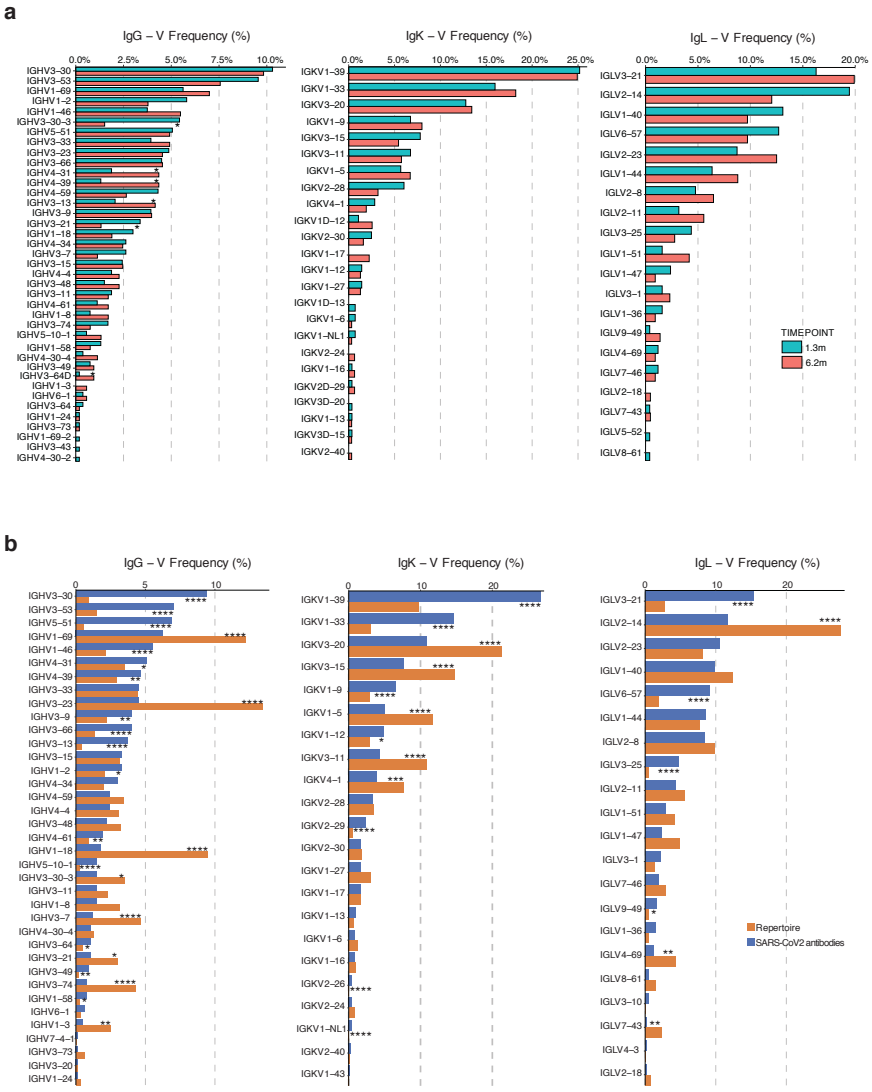

682

683 **Extended Data Fig. 4: Frequency distributions of human V genes.**

684 **a,** Two-sided binomial tests were used to compare the frequency distributions of human V genes

685 of anti-SARS-CoV-2 antibodies from donors at 1.3 months to 6.2 months [1]. **b,** Two-sided binomial

686 tests were used to compared the frequency distributions of human V genes of anti-SARS-CoV-2

687 antibodies from this study to sequence from *C. Soto et al.* [49].

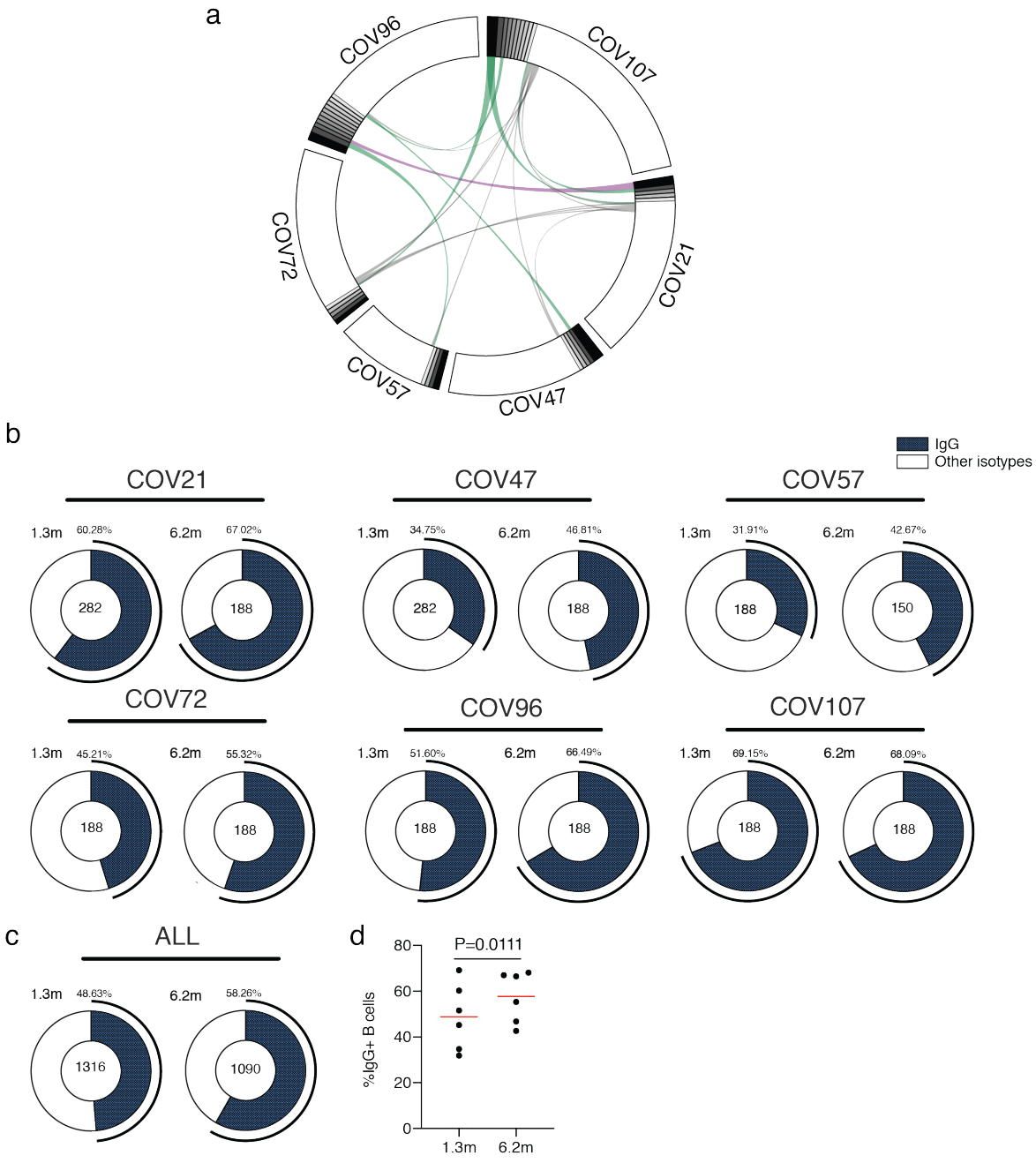

688

689 **Extended Data Fig. 5: Circos plots and IgG positive RBD specific B cells**

690 **a,** Sequences from all six individuals with clonal relationships depicted as in Figure 2d.
691 Interconnecting lines indicate the relationship between antibodies that share V and J gene segment
692 sequences at both IGH and IGL. Purple, green and grey lines connect related clones, clones and
693 singles, and singles to each other, respectively. **b,** For each patient, the number of IgG heavy chain

694 sequences (black) analyzed from six individuals at month 1.3 (left panel) or month 6.2 post-
695 infection (right panel). The number in the inner circle indicates the number of cells that was sorted
696 for each individual denoted above the circle. **c,** The same as b but showing the all 6 patients
697 combined data. **d,** The comparison of the percentage of IgG positive B cells from six individuals
698 at month 1.3 or month 6.2 post-infection. The horizontal bars indicate the mean. Statistical
699 significance was determined using paired t test.

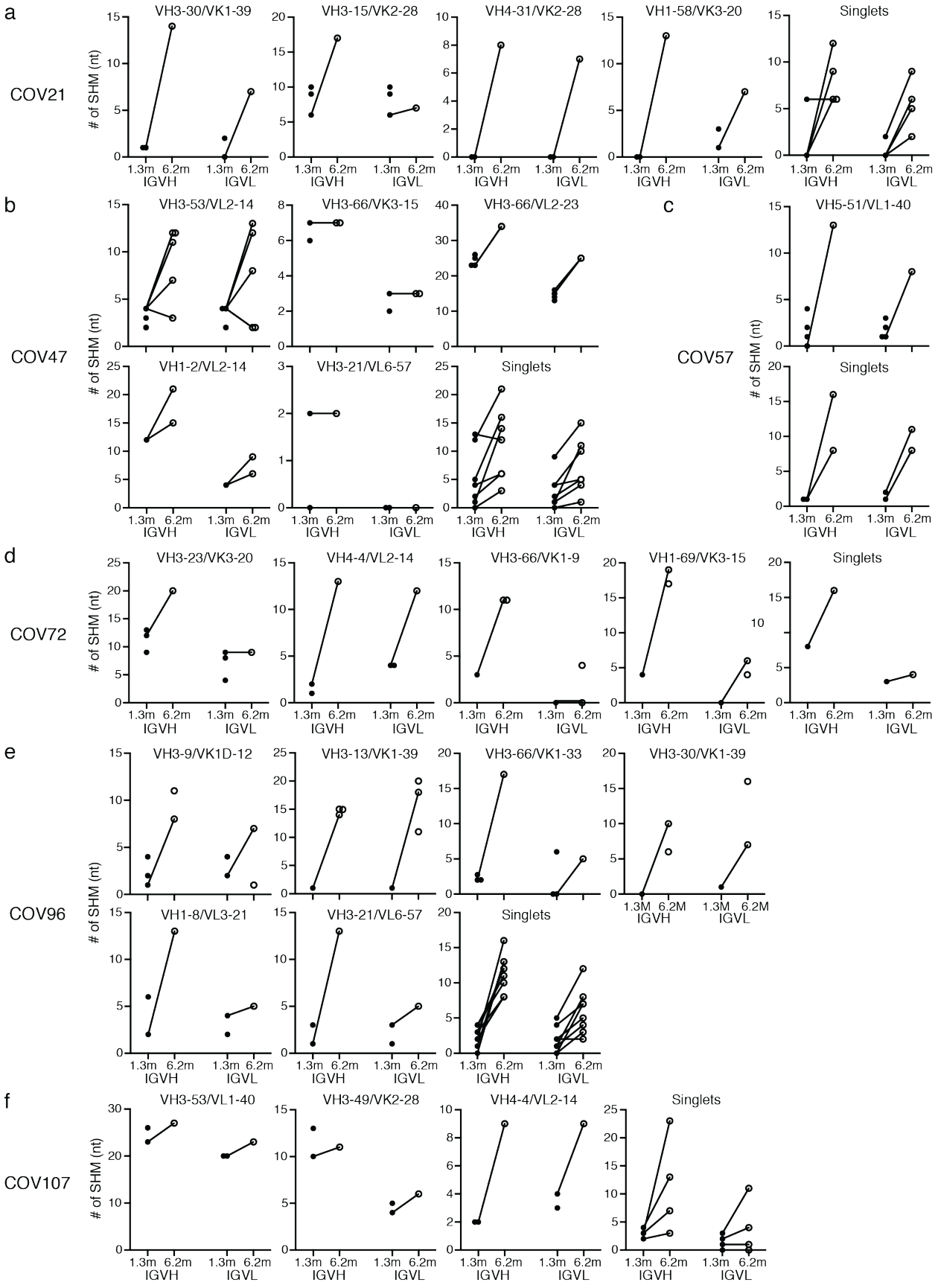

Extended Data Fig. 6: Analysis of antibody somatic hypermutation of persisting clones.

Number of somatic nucleotide mutations in both the IGVH and IGVL of persisting clones found at month 1.3 (solid circles) and month 6.2 time points (open circles) in patients (a) COV21, (b) COV47, (c) COV57, (d) COV72, (e) COV96, and (f) COV107. The VH and VL gene usage of each clonal expansion is indicated above the graphs, or are indicated as “Singlets” if the persisting sequence was isolated only once at both time points. Connecting line indicates the SHM of the clonal pairs that were expressed as a recombinant mAbs.

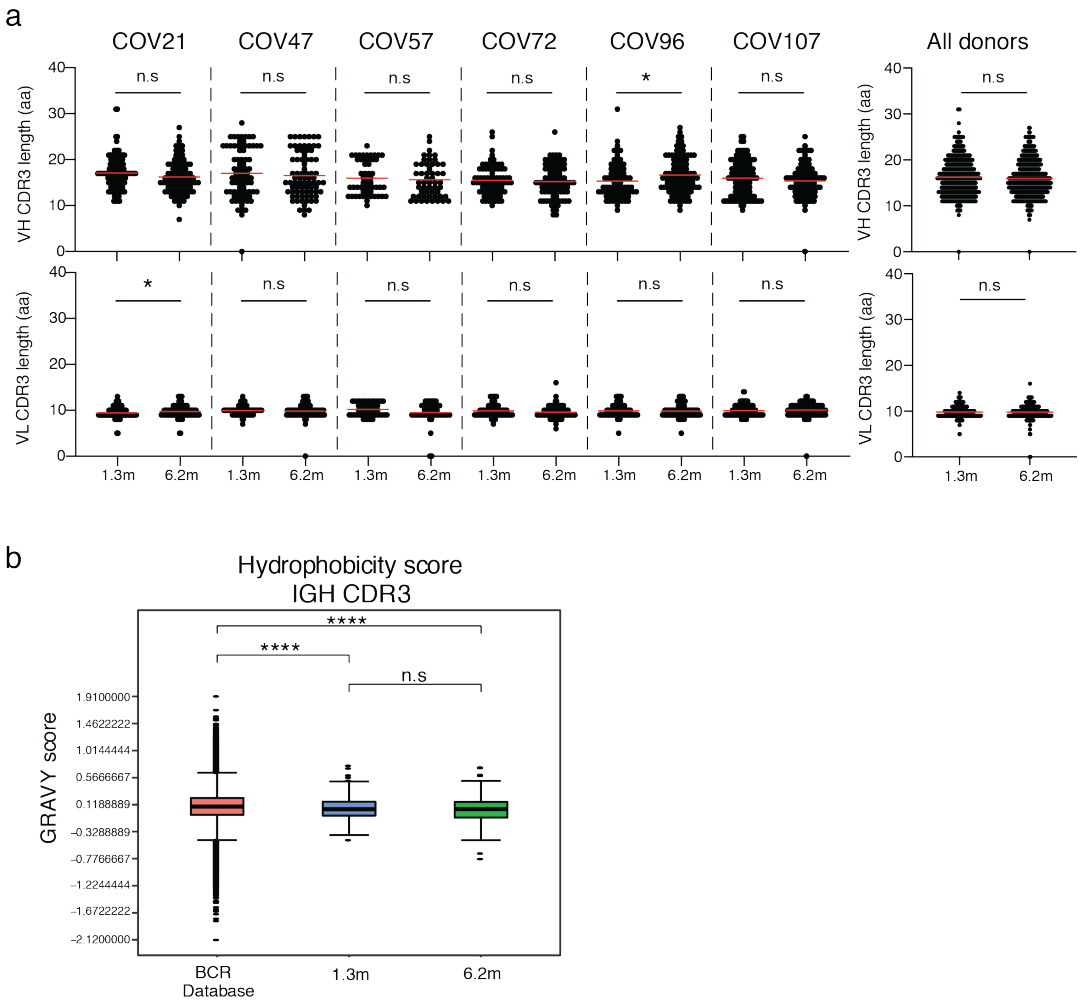

Extended Data Fig. 7: Analysis of CDR3 length and hydrophobicity.

a, For each individual, the number of the amino acid length of the CDR3s at the IGVH and IGVL is shown. The horizontal bars indicate the mean. The number of antibody sequences (IGVH and IGVL) evaluated for each participant are n = 90 (COV21), n = 78 (COV47), n = 53 (COV57), n = 87 (COV72), n = 104 (COV96), n = 120 (COV107). Right panel show all antibodies combined (n = 532 for both IGVH and IGVL). **b,** Distribution of the hydrophobicity GRAVY scores at the IGH CDR3 in antibody sequences from this study compared to a public database (see Methods for statistical analysis). The box limits are at the lower and upper quartiles, the centre line indicates the median, the whiskers are 1.5× interquartile range and the dots represent outliers.

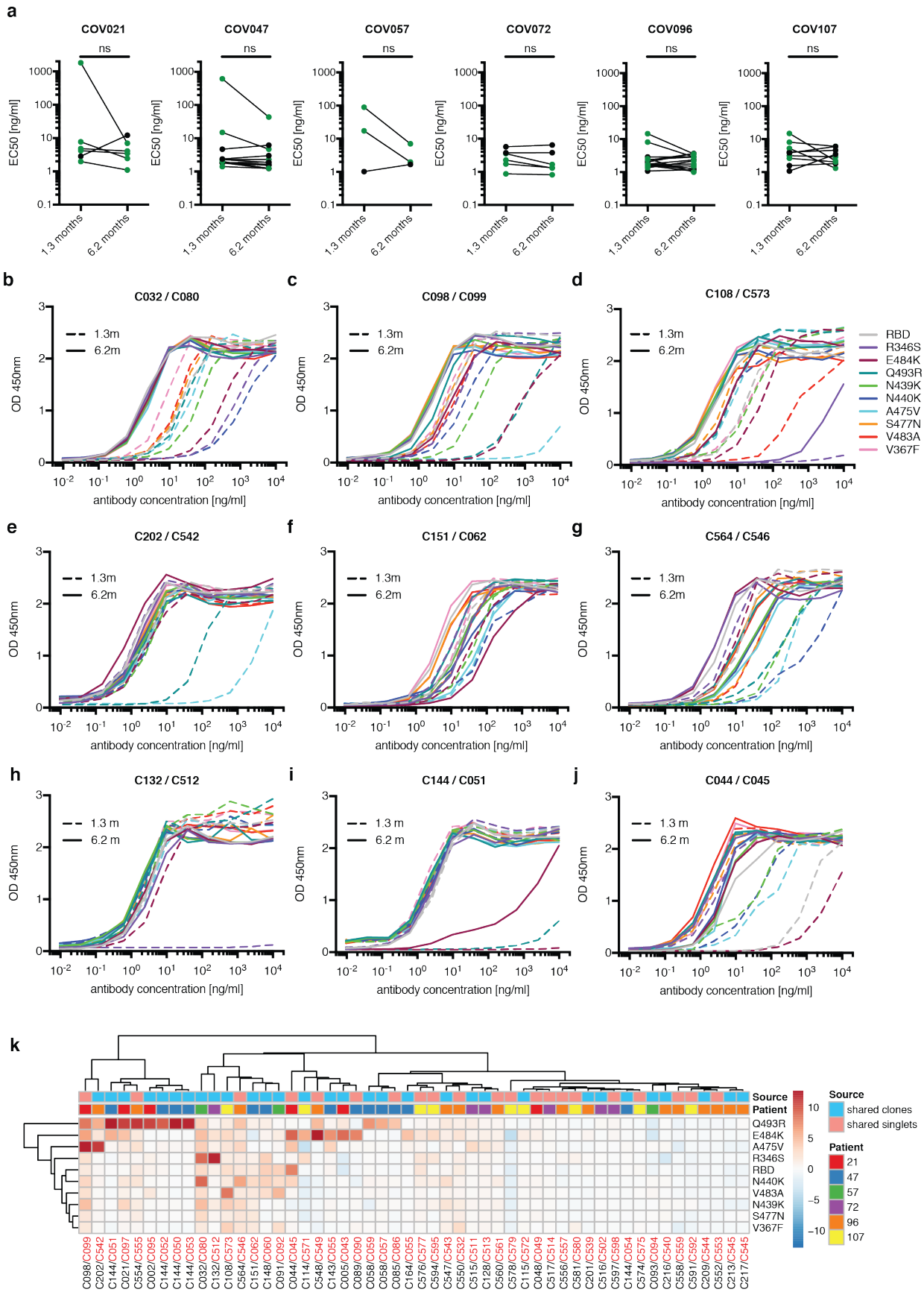

719

Extended Data Fig. 8: ELISA of wt/mutant RBD for mAbs.

a, EC50 values for binding to wild type RBD of shared singlets and shared clones of mAbs obtained at the initial 1.3 and 6.2 months follow-up visit, divided by patient. Lines connect shared singlets/clones. mAbs with improved EC50 at 6.2 months follow-up visit are highlighted in green, remaining mAbs are shown in black. Statistical significance was determined using Wilcoxon matched-pairs signed rank test. **b-j,** Graphs show ELISA binding curves for different antibodies obtained at 1.3 months (dashed lines) and their clonal relatives obtained after 6.2 months (solid lines) binding to wild type, R346S, E484K, Q493R, N439K, N440K, A475V, S477N, V483A and V367F RBDs (colors as indicated). Antibody IDs of pairs as indicated on top of panels (1.3m / 6.2m). **k,** Heat map shows log2 relative fold change in EC_{50} against the indicated RBD mutants for 52 antibody clonal pairs obtained at 1.3 (black) and 6.2 months (red). The clonal and participant origin for each antibody pair is indicated above.

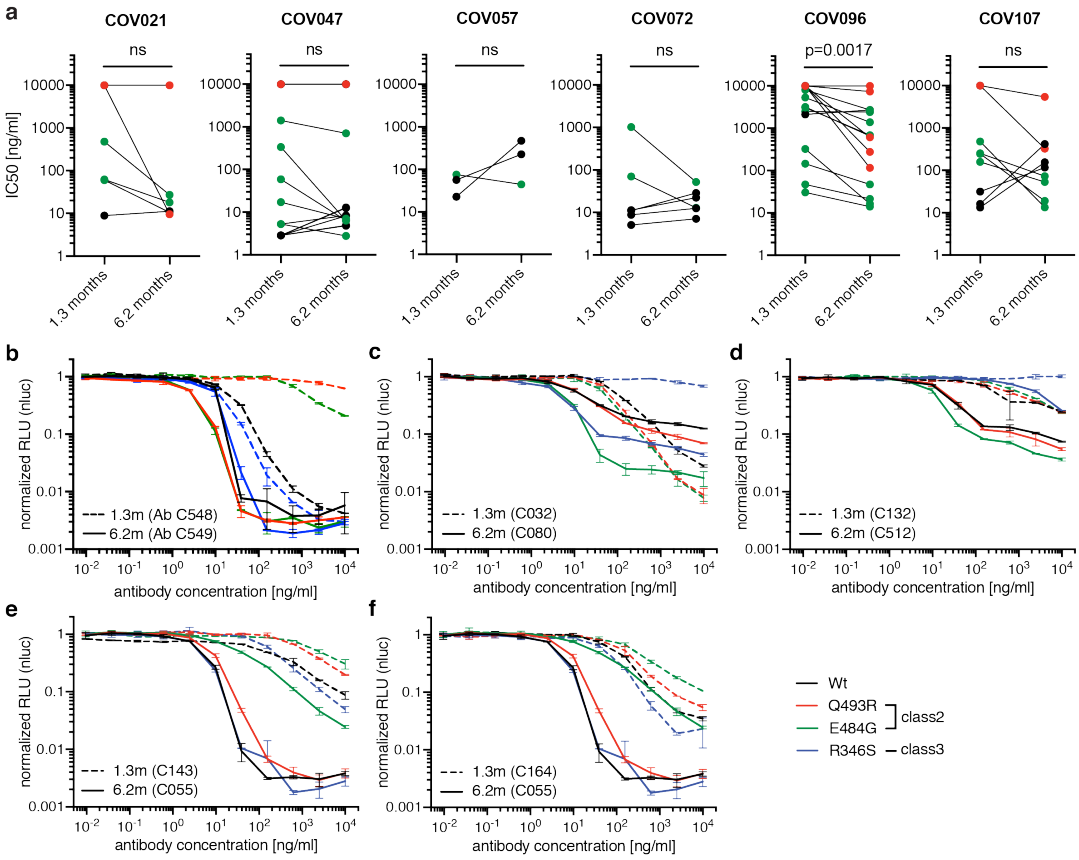

732

733 **Extended Data Fig. 9: neutralization of wt/mutant RBD pseudotypes by mAbs.**

734 **a,** IC50 values of shared singlets and shared clones of mAbs obtained at the initial 1.3- and 6.2-
735 months follow-up visit, divided by patient. Lines connect shared singlets/clones. mAbs with
736 undetectable IC50 at 1.3 months are plotted at 10 µg/ml and are highlighted in red, mAbs with
737 improved IC50 at 6.2 months follow-up visit are highlighted in green, remaining mAbs are shown
738 in black. Statistical significance was determined using Wilcoxon matched-pairs signed rank test.
739 **b-f,** The normalized relative luminescence values for cell lysates of 293TAce2 cells 48 hpi with
740 SARS-CoV-2 pseudovirus harboring wt RBD or RBD-mutants (wt, Q493R, E484G and R346S
741 RBD shown in black, red, green and blue, respectively) in the presence of increasing
742 concentrations of mAbs obtained at the 1.3 months initial visit (1.3m, dashed lines) and their shared
743 clones/singlets at the 6.2 follow-up visit (6.2m, continuous lines). Antibody IDs as indicated.

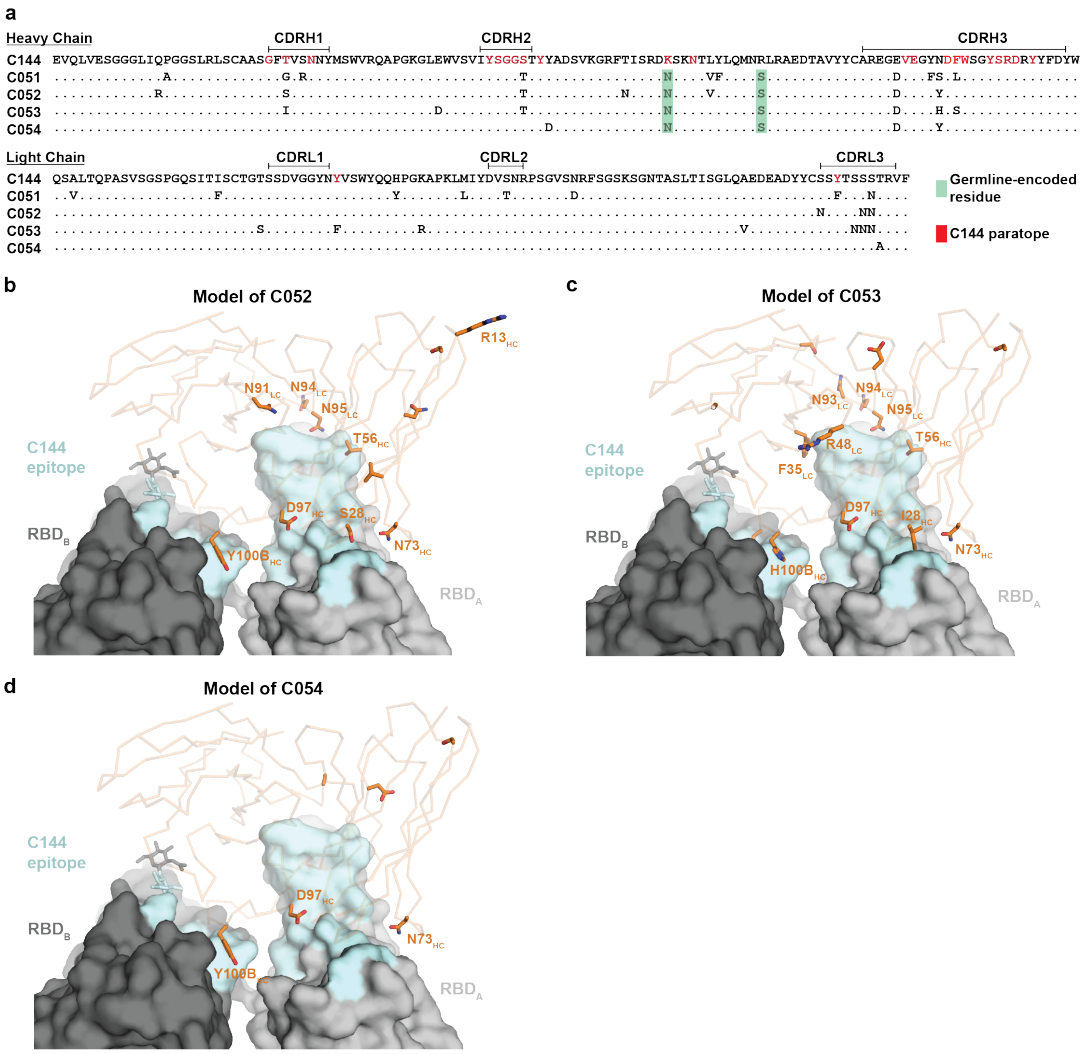

Extended Data Fig. 10: C51 alignment and binding projection

a, VH and VL amino acid sequence alignment of C144 and derivative antibodies C051, C052, C053 and C054. Germline-encoded residues are highlighted in green. Residues in the proximity of RBD-binding C144 paratope are highlighted in red.

b-e, Surface representation of two adjacent "down" RBDs (RBD_A and RBD_B) on a spike trimer with the C144 epitope on the RBDs highlighted in cyan and positions of amino acid mutations that accumulated in **b,** C052. **c**, C053 and **d**, C054 compared to the parent antibody C144 highlighted as stick side chains on a Cα atom representation. The C052, C053 and C054 interactions with two RBDs was modeled based on a cryo-EM structure of C144 Fab bound to spike trimer [16].

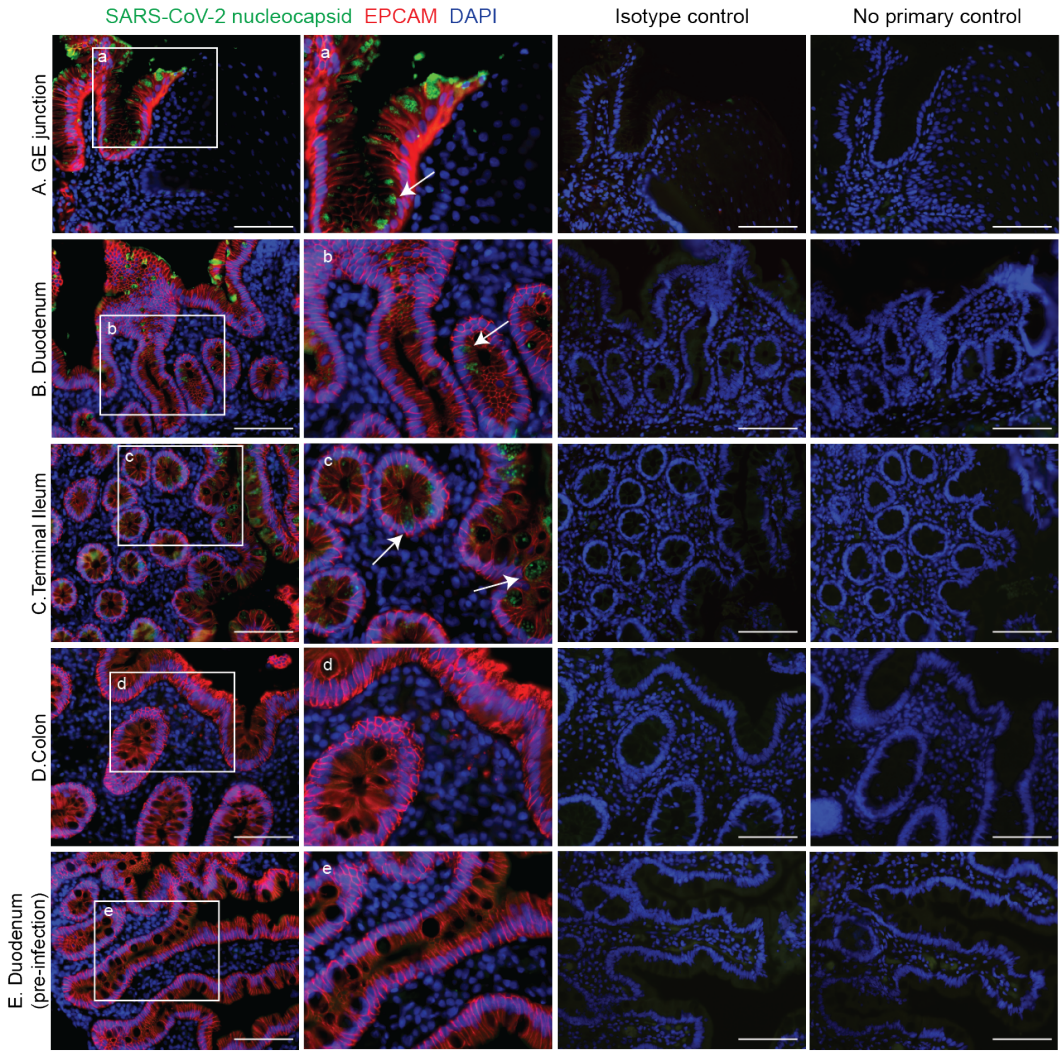

754

755 **Extended Data Fig. 11**: **SARS-CoV-2 antigen in human enterocytes in the gastrointestinal**

756 **tract 3 months post COVID-19**

757 Immunofluorescence images of human gastrointestinal tissue are shown. Staining is for EPCAM

758 (red), DAPI (blue) and SARS-CoV-2 nucleocapsid (green) Samples are derived from intestinal

759 biopsies in the gastrointestinal tract as indicated (A-E). (A-D) are biopsies from participant CGI-

760 088 (Supplementary Table 7) taken 92 days post COVID-19 symptom onset. (E) is a biopsy 27

761 months prior to COVID-19 symptom onset from the same participant CGI-088. Arrows indicate

762 enterocytes with detectable SARS-CoV-2 antigen. Isotype and no primary controls for each tissue

763 are shown in the last two columns. White scale bar corresponds to 100 μm.

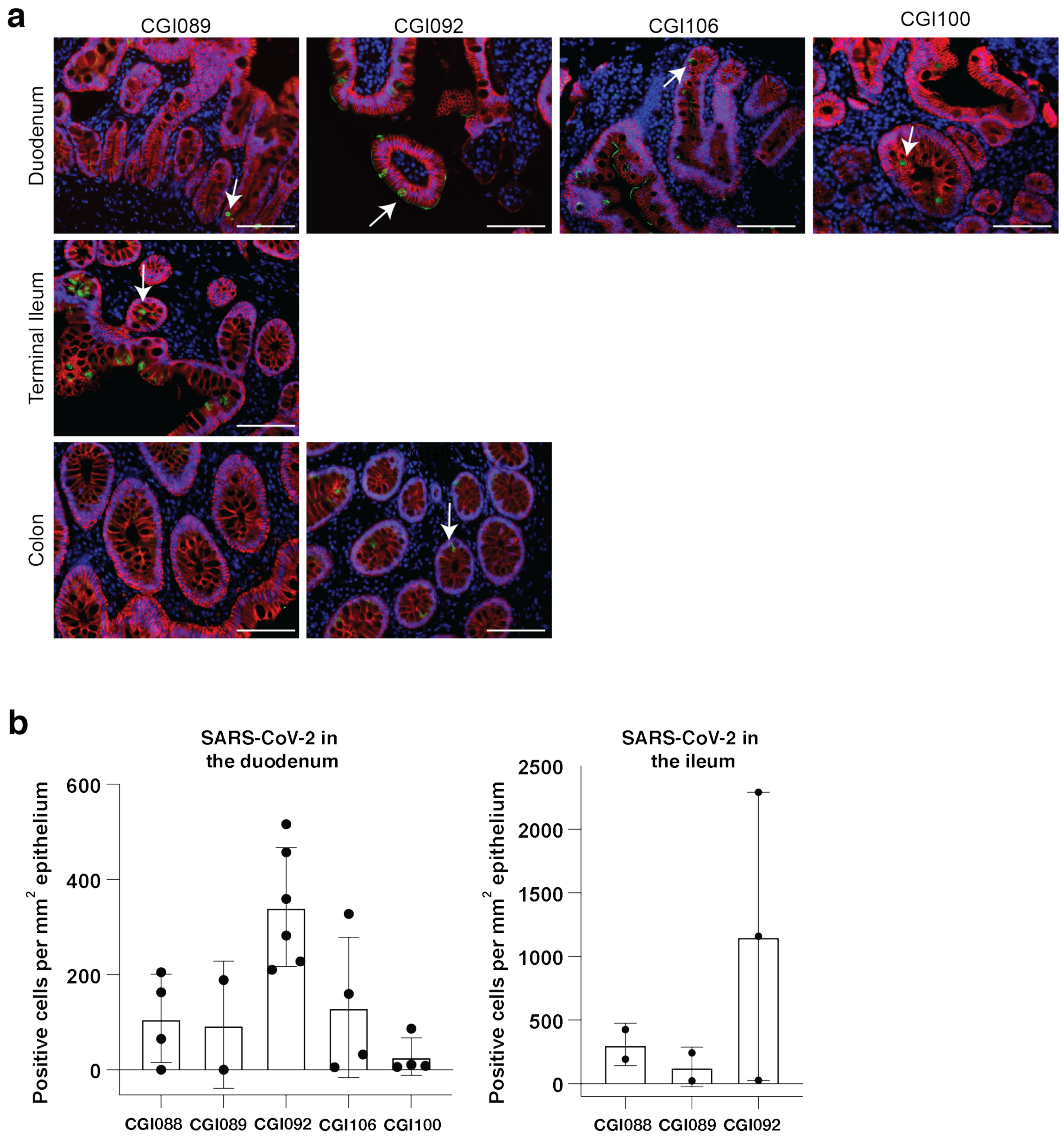

764

765 **Extended Data Fig. 12**: **SARS-CoV-2 antigen is detectable in different intestinal segments in**

766 **multiple COVID-19 convalescent individuals**

767 **a**, Immunofluorescence (IF) images of biopsy samples in the gastrointestinal tract in different

768 individuals are shown. Staining is for EPCAM (red), DAPI (blue) and SARS-CoV-2 nucleocapsid

769 (green). Samples are derived from intestinal biopsies from 4 participants (CGI089, CGI092,

770 CGI100 and CGI106) taken at least 3 months after COVID-19 infection. Arrows indicate

771 enterocytes with detectable SARS-CoV-2 antigen. White scale bar corresponds to 100 μm. **b**,

772 Quantification of SARS-CoV-2 positive cells by immunofluorescence. The number of cells
773 staining positive for the nucleocapsid protein (N) of SARS-CoV-2 per mm^2 of intestinal epithelium
774 is shown. The graphs show biopsy samples from the indicated individuals of the duodenum (left)
775 and terminal ileum (right), respectively. Black dots represent the number of available biopsy
776 specimen for each individual from the respective intestinal segment. Boxes represent median
777 values and whiskers the 95 % CI.

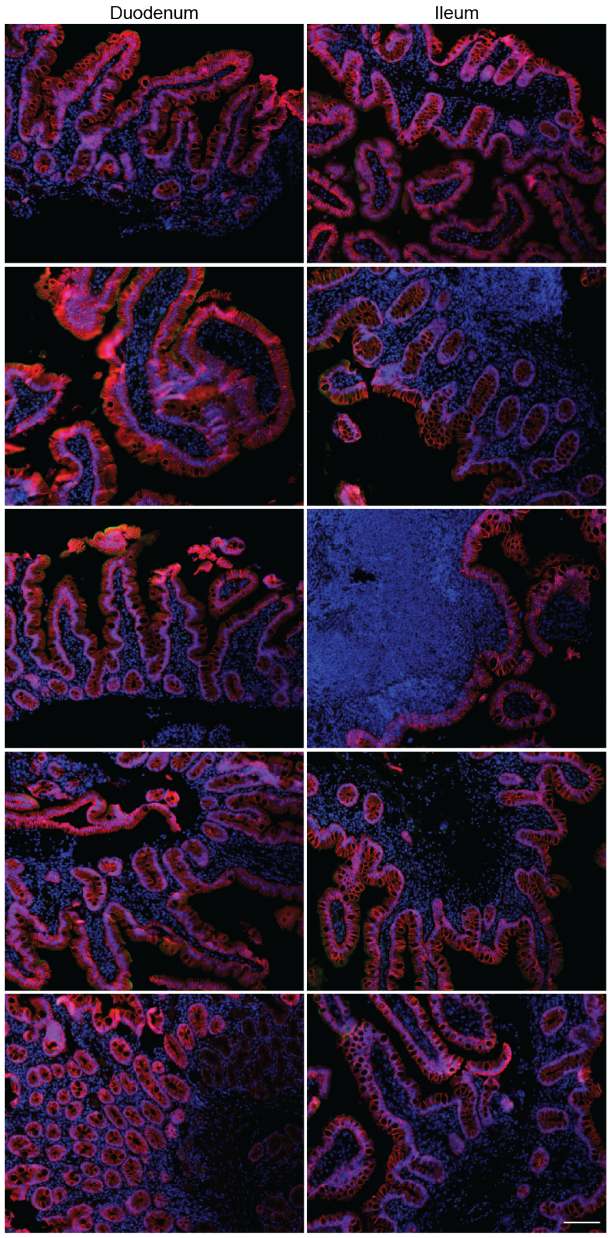

778

779 **Extended Data Fig. 13: Pre-COVID-19 historic control individuals show no detectable**
780 **SARS-CoV-2 antigen by immunofluorescence**

781 Immunofluorescence images of biopsy samples in the gastrointestinal tract obtained from 10
782 different individuals between January 2018 and October 2019 are shown. Staining is for EPCAM
783 (red), DAPI (blue) and SARS-CoV-2 nucleocapsid (green). White scale bar corresponds to 100
784 μm.

785

Supplementary Tables

Table S1. Cohort characteristics

			Temporal dynamics (days)					ELISA binding								Neutralization (NT50)	
								RBD (AUC)						N (COI)			
Sex	n	Age (years)	Sx onset to initial visit (T1)	Sx onset to follow-up visit (T2)	Time between visits	Acute disease severity by WHO (0-8) ¶	Post-acute Sx persistence †	IgG (T1)	IgG (T2)	IgM (T1)	IgM (T2)	IgA (T1)	IgA (T2)	total Ig (T1)	total Ig (T2)	(T1)	(T2)
Male	52	44.5 (24-76)	39 (21-63)	190 (165-211)	148 (119-178)	2 (0-6)	25/52 (48.1 %)	11632	6697	2811	1502	1411	1218	47.8	53.9	649	78
Female	35	45 (26-73)	36 (17-67)	192 (168-223)	154 (122-179	2 (0-5)	13/35 (37.1 %)	8884	6834	2358	1459	1235	1083	59.8	56.8	297	87

Sx = Symptoms
¶ = WHO Ordinal Scale for Clinical Improvement, COVID-19 Trial Design Synopsis
† = Persistent fatigue, dyspnea, athletic deficit, or ≥ 3 other solicited symptoms beyond 6 weeks from Sx onset
Reported data are median (range) unless stated otherwise

Supplementary Table 1: Cohort summary

SI Table 1. Individual participant characteristics

					Temporal dynamics (days)							Serological assays												Neutralization (NT50)	
												RBD (AUC)						RBD (Pylon, IV)				N (COI)			
ID	Age (years)	Sex	Race	Ethnicity	Sx duration during acute disease	Sx onset to initial visit (T1)	Sx onset to follow-up visit (T2)	Time between visits	# of solicited comorbidities §	Acute disease severity by WHO (0-8) ¶	Post-acute Sx persistence †	IgG (T1)	IgG (T2)	IgM (T1)	IgM (T2)	IgA (T1)	IgA (T2)	IgG (T1)	IgG (T2)	IgM (T1)	IgM (T2)	total Ig (T1)	total Ig (T2)	(T1)	(T2)
7	40	M	White	Non-Hispanic	11	30	181	151	0	2	Y	11981	9545	6524	1516	1479	1344	34	18	3.6	0.31	56	171	2730	192
8	37	M	White	Non-Hispanic	3	57	205	148	0	2	Y	9010	7653	1998	1153	1342	1380	6.9	4.9	0.27	0.26	43	16	151	39
9	35	F	White	Non-Hispanic	12	53	201	148	0	2	Y	18953	12848	2963	1753	989	1227	27	23	1.1	0.49	174	187	306	295
20	26	F	White	Non-Hispanic	2	17	191	174	1	2	N	4134	8690	1976	1228	1018	1314	1.5	13	0.36	0.25	1	4	50	172
21	54	M	White	Hispanic	11	27	200	173	1	2	Y	36389	20744	14506	1242	2855	1914	127	59	4.4	0.23	82	159	5053	561
24	34	M	White	Non-Hispanic	15	30	175	145	1	1	N	5736	3803	2715	1150	927	1101	2.9	0.93	0.34	0.2	6	17	281	10
27	28	M	White	Non-Hispanic	9	32	210	178	1	1	Y	9283	5312	2182	1943	2182	1943	13	4.5	0.35	0.21	88	168	739	86
31	51	M	White	Non-Hispanic	9	33	183	150	0	2	Y	3212	3705	1272	903	906	913	1.3	1.5	0.22	0.15	35	41	192	18
38	57	F	White	Non-Hispanic	10	38	211	173	0	2	N	13718	12760	2009	1249	2902	3198	11	5.9	0.24	0.35	49	35	519	832
40	44	M	White	Non-Hispanic	7	23	195	172	0	2	N	5291	6467	1792	1161	1481	1501	0.6	0.6	0.33	0.15	3	12	64	10
46	39	M	White	Non-Hispanic	8	30	174	144	0	2	Y	4799	4416	2247	1315	1055	1153	3	2.2	0.24	0.17	51	141	59	21
47	43	F	White	Non-Hispanic	11	33	177	144	0	2	Y	17581	9284	9749	1914	1586	851	43	16	1.2	0.21	103	101	10433	349
48	37	F	White	Non-Hispanic	7	21	174	153	0	2	N	3265	3681	2358	1952	802	898	2.8	3.9	0.27	0.23	2	10	173	22
55	36	M	White	Non-Hispanic	3	49	210	161	0	2	N	12982	6419	2515	1487	2213	1466	16	3.3	0.27	0.19	85	17	186	10
57	66	M	White	Non-Hispanic	6	21	180	159	4	2	N	9108	4987	9199	2622	954	884	23	4.6	1.7	0.35	19	128	2049	45
71	45	F	White	Non-Hispanic	12	48	202	154	0	2	Y	5207	4559	1606	998	723	860	3.5	6.6	0.14	0.33	21	33	112	65
72	42	M	White	Non-Hispanic	16	35	188	153	1	2	Y	24822	10485	24034	2095	4887	2407	N/A	N/A	N/A	N/A	N/A	N/A	3138	81
75	46	F	White	Non-Hispanic	10	36	212	176	0	1	N	5083	3811	1386	1459	1386	1459	7.2	2.1	0.36	0.2	71	74	271	36
76	49	F	White	Non-Hispanic	28	34	204	170	0	1	Y	8354	5632	1697	1299	1320	886	5.1	0.67	0.23	0.22	3	2	220	10
82**	46	M	N/A	Non-Hispanic	0	N/A	N/A	163	0	1	N	6472	5187	2667	3094	1125	846	N/A	N/A	N/A	N/A	N/A	N/A	131	20
88	41	M	White	Non-Hispanic	7	23	180	157	1	1	N	8263	6730	1789	2276	1546	903	4.7	9.3	0.56	0.31	7	186	425	56
95	44	M	White	Non-Hispanic	9	36	204	168	1	2	Y	14380	7894	2709	1703	1250	1023	18	7.2	0.42	0.12	136	235	962	155
96	48	F	White	Non-Hispanic	9	30	194	164	0	1	N	24147	15675	3959	1498	1099	965	N/A	N/A	N/A	N/A	N/A	N/A	928	206
98	35	F	White	Non-Hispanic	2	24	203	179	0	2	N	8275	7190	2495	2417	2495	2417	15	6.9	0.7	0.65	72	55	249	53
99	36	F	White	Non-Hispanic	13	29	204	175	0	2	N	12764	6017	2693	2390	2693	2390	24	5.3	0.41	0.34	46	12	1128	163
107	53	F	White	Non-Hispanic	10	29	202	173	0	2	Y	7967	8298	1560	1525	915	850	3.8	6.3	0.49	0.18	64	76	297	87
114	30	F	White	Non-Hispanic	15	36	195	159	0	2	Y	5979	5654	1163	912	898	940	N/A	N/A	N/A	N/A	N/A	N/A	114	32
115	65	F	White	Non-Hispanic	20	41	188	147	0	2	N	26997	11600	19944	2081	991	890	63	22	2.9	0.27	116	157	1128	432
119	56	M	White	Non-Hispanic	13	48	207	159	0	1	N	12155	6663	7000	1533	2152	1822	13	4.2	14	1.1	20	23	650	35
120	56	F	White	Non-Hispanic	26	48	207	159	0	1	N	8096	3292	2310	1091	856	1145	5.5	2.7	0.33	0.14	10	9	101	10
123	26	M	White	Non-Hispanic	12	34	191	157	0	2	Y	5977	6228	2722	1880	1127	1357	2.1	0.67	0.21	0.15	4	2	76	10
125	51	F	White	Non-Hispanic	10	26	168	142	0	1	N	4498	4271	2234	1361	684	807	1.8	1.1	1	0.19	4	2	127	10
131	39	M	White	Non-Hispanic	5	25	191	166	0	0	N	4285	3911	1318	943	1201	1166	0.27	0.93	0.35	0.26	1	3	50	14
132	36	M	White	Non-Hispanic	10	50	193	143	0	0	N	12506	8783	8532	4822	1068	1070	10	9.8	0.81	0.26	161	149	521	200
134	27	F	White	Non-Hispanic	16	22	171	149	0	0	N	8884	6818	7472	2068	1057	982	4.1	3.7	2.1	0.37	15	6	2701	263
135	62	F	White	Non-Hispanic	8	31	190	159	0	2	N	9301	8386	3157	888	1256	952	9.9	16	0.77	0.21	50	81	350	441
140	63	F	White	Non-Hispanic	28	47	223	176	0	1	N	6181	4957	1235	1061	1235	1061	3.5	2.2	0.22	0.12	39	14	52	13
149	41	M	White	Non-Hispanic	17	28	173	145	1	2	N	6275	3875	1422	1073	1058	842	10	3.4	0.48	0.21	69	151	495	28
154	68	M	Asian	Non-Hispanic	16	30	196	166	3	2	Y	25056	13409	5544	1169	2072	1205	57	16	2.9	0.18	13	23	928	65
157	50	M	White	Non-Hispanic	10	32	179	147	0	1	N	11979	8751	11125	2370	1969	1374	15	7.9	5.4	0.71	67	89	742	190
172	38	F	White	Non-Hispanic	8	22	182	160	1	2	N	10507	6124	4007	1339	3230	1244	5.2	5.1	0.85	0.21	14	102	301	157
173	47	M	White	Non-Hispanic	5	53	185	132	0	2	N	9127	5004	12194	1660	1162	979	2.5	2.8	7.3	0.59	149	143	647	176
178	26	F	White	Non-Hispanic	6	24	190	166	1	1	N	4316	3757	1394	1373	1351	1222	1.2	0.73	0.43	0.49	2	3	10	10
186	38	F	N/A	N/A	8	33	189	156	0	1	N	7427	4850	1687	960	1085	815	10	5	0.41	0.29	64	32	297	73
190*	54	F	White	Non-Hispanic	18	63	190	127	0	4	Y	16156	10408	4567	1664	1207	1107	43	18	0.9	0.42	102	81	598	165
192*	47	F	White	Non-Hispanic	44	62	190	128	1	3	Y	13879	9000	5894	1525	1819	1598	30	22	0.68	0.38	106	145	608	409
195	24	M	White	Non-Hispanic	18	42	191	149	0	2	N	14242	7933	3954	2055	1227	978	22	6.9	1.5	0.24	15	31	1315	106
201	50	M	White	Non-Hispanic	15	33	185	152	1	2	N	26093	11284	6230	1635	3374	1477	131	48	3.3	0.23	34	69	3897	741
222	28	M	Asian	Non-Hispanic	11	37	173	136	1	2	N	14063	6930	1132	723	2841	1612	7.9	2.7	0.37	0.18	14	17	865	50
229	45	M	White	Non-Hispanic	10	63	203	140	1	2	N	14677	8054	5507	1606	1066	1141	31	19	0.49	0.25	146	191	1273	135
230	50	M	White	Non-Hispanic	18	33	190	157	0	2	Y	5605	3015	1300	1868	1059	1130	1.8	1.5	0.19	0.17	6	10	382	375
232	38	F	White	Non-Hispanic	13	43	197	154	1	2	N	8127	15997	1948	2352	1335	1362	N/A	N/A	N/A	N/A	N/A	N/A	147	633
233	55	M	White	Non-Hispanic	20	41	206	165	0	2	N	6897	6940	1917	1211	1066	1065	8.3	4.3	0.27	0.16	3	9	173	11
241	36	M	White	Non-Hispanic	12	30	202	172	1	2	N	8912	5749	7327	1446	2562	2195	3.3	0.8	1.4	0.38	69	18	923	118
256	63	F	White	Non-Hispanic	27	42	217	175	0	2	Y	10574	6500	1886	1533	1886	1533	7.7	6.4	0.34	0.17	65	27	142	31
287	47	M	White	Non-Hispanic	11	23	165	142	0	1	N	7442	4357	2873	1211	910	928	9.3	3.9	0.77	0.41	15	15	240	38
310	34	F	White	Non-Hispanic	17	35	185	150	0	2	Y	26782	15634	1554	1023	1435	1083	47	15	0.27	0.31	51	137	485	153
314	46	M	White	Non-Hispanic	11	43	184	141	0	2	Y	12475	7247	2431	1273	854	811	38	14	0.89	0.2	131	198	667	297
315	29	F	White	Non-Hispanic	15	42	190	148	0	1	N	18570	13153	2528	2022	1252	1083	55	21	0.75	0.31	135	58	376	179
319	50	M	White	Non-Hispanic	5	38	180	142	1	2	N	7614	4736	2215	762.1	1575	1174	6.9	3.9	0.26	0.16	27	12	241	74
323	39	F	White	Non-Hispanic	7	45	185	140	0	2	N	4220	5152	2930	1547	888	931	0.93	0.67	0.33	0.34	4	1	51	20
325	52	M	White	Non-Hispanic	16	38	192	154	0	2	Y	26673	12400	16598	4879	2703	1464	54	14	14	3	50	56	1603	229
328	54	F	White	Non-Hispanic	22	62	203	141	0	2	N	8118	7073	1216	1268	1216	1268	7.5	5.5	0.29	0.21	99	81	94	66
352	44	M	White	Non-Hispanic	16	43	197	154	0	2	N	19958	6525	5585	1064	2614	1731	43	11	0.84	0.22	17	16	519	33
353	60	M	White	Non-Hispanic	14	49	186	137	0	2	Y	23981	13736	6807	2062	9230	3637	58	20	0.83	0.22	68	51	855	222
393*	69	M	White	Non-Hispanic	23	54	187	133	0	5	N	8729	5150	13320	1974	1075	892	14	6.1	2.5	0.27	13	51	715	144
394	48	F	Multiple	Hispanic	7	67	200	133	2	2	N	22856	12823	6178	1909	1009	1131	96	35	1.1	0.34	59	69	1281	282
401	61	M	White	Non-Hispanic	16	53	209	156	0	2	Y	31108	19746	1677	1336	1677	1336	94	34	4.8	0.4	89	118	1098	134
403*	52	M	Asian	Non-Hispanic	18	39	174	135	1	4	Y	24462	13614	4060	3187	2107	1164	170	29	0.7	0.13	29	41	3888	179
410	34	M	White	Non-Hispanic	12	46	192	146	1	2	Y	6355	4353	2456	1730	1249	1112	2.8	1.3	0.36	0.29	25	19	222	65
437	43	F	Asian	Non-Hispanic	14	34	192	158	1	2	N	15987	6834	3051	1940	3051	1940	16	6.3	0.89	0.23	146	75	699	176
461	49	M	White	Non-Hispanic	7	39	185	146	2	2	Y	17491	13418	6867	1946	1827	1454	38	44	2	0.46	73	182	1077	361
470	28	F	White	Non-Hispanic	17	51	173	122	0	2	Y	6054	4894	2315	1798	1003	1025	5.3	3.1	0.2	0.16	90	86	50	14
478	31	M	White	Non-Hispanic	16	52	172	120	0	1	Y	6600	4083	3238	1824	1264	1283	7.1	3.3	1.8	0.24	33	41	263	15
500	46	M	White	Non-Hispanic	12	53	207	154	0	2	N	6039	5366	2254	2305	2356	2412	4.2	1.6	0.57	0.2	26	16	194	36
501*	32	M	Asian	Non-Hispanic	18	53	192	139	0	4	Y	22775	8667	5272	1242	1557	1098	N/A	N/A	N/A	N/A	N/A	N/A	719	125
506	46	M	White	Non-Hispanic	12	59	178	119	1	2	Y	3036	2595	1205	975	1338	1041	N/A	N/A	N/A	N/A	N/A	N/A	10	10
507	39	M	White	Non-Hispanic	15	60	200	140	0	2	Y	15458	7586	4505	989	1208	1218	22	13	0.88	0.36	104	90	400	49
509	36	M	White	Non-Hispanic	11	50	190	140	0	2	N	9217	5538	2930	1258	1286	1417	11	4.5	0.41	0.18	165	189	236	36
537	52	M	White	Non-Hispanic	15	45	178	133	2	2	Y	11285	6443	2448	1083	1245	1192	13	8.6	0.56	0.23	89	52	923	986
539*	73	F	White	Non-Hispanic	19	55	209	154	1	5	Y	20337	9568	7505	1386	1714	2124	68	41	1	0.65	144	199	488	50
547*	59	M	White	Non-Hispanic	15	36	211	175	0	3	N	28228	15394	3863	2048	3863	2048	73	33	9.1	0.22	66	140	2901	211
632	38	M	White	Non-Hispanic	10	43	168	125	0	2	Y	16796	9152	1766	1548	2415	1833	31	12	0.36	0.25	141	153	572	161
633	39	M	White	Non-Hispanic	8	57	182	125	0	1	N	8759	5108	1436	1224	2019	1404	4.8	3.3	0.25	0.26	121	157	135	32
652*	76	M	White	Non-Hispanic	18	56	211	155	2	6	N	25025	7388	2748	1433	2748	1433	112	27	1	0.18	79	73	2324	275
664*	45	F	White	Non-Hispanic	17	42	192	150	0	5	Y	12698	6927	3357	1420	1440	1395	11	4	0.43	0.21	61	26	384	37
674*	41	M	White	Non-Hispanic	17	57	182	125	0	4	Y	36682	21702	3061	1141	1320	1218	251	57	0.4	0.13	45	66	1619	298

Sx = symptoms
* = hospitalized, **=asymptomatic
§ = Arterial hypertension (HTN), obesity (OB), diabetes mellitus (DM), asthma (A), chronic obstructive pulmonary disease (COPD), coronary artery disease (CAD), cancer (CX)
¶ = WHO Ordinal Scale for Clinical Improvement, COVID-19 Trial Design Synopsis
† = Persistent fatigue, dyspnea, athletic deficit, or ≥ 3 other solicited symptoms beyond 6 weeks from Sx onset
Reported data are median (range) unless stated otherwise

Supplementary Table 2: Individual participant characteristics

791 **Supplementary Table 3: Antibody sequences from 1.3 and 6.2 month time point is provided**

792 **as a separate Excel file.**

793 **Supplementary Table 4: Sequences of the cloned monoclonal antibodies is provided as a**

794 **separate Excel file.**

795 **Supplementary Table 5: Half maximal effective concentrations (EC50s) of the monoclonal**

796 **antibodies is provided as a separate Excel file.**

797 **Supplementary Table 6: Inhibitory concentrations of the monoclonal antibodies is provided**

798 **as a separate Excel file.**

SI Table 7. Gastrointestinal cohort participant characteristics

	Baseline patient characteristics						Gastrointestinal endoscopy				SARS-CoV-2 in the intestine					COVID-19 history					
											SARS-CoV-2 nucleocapsid (N) antigen by immunofluorescence (IF)		Corona virion-like particles by electron microscopy (EM)	SARS-CoV-2 qPCR from intestinal biopsy samples		Positive nasopharyngeal SARS-CoV-2 PCR	Positive SARS-CoV-2 serology	Symptom onset to GI biopsy (days)	Positive nasopharyngeal PCR to GI biopsy (days)	Acute disease severity by WHO (0-8) ¶	COVID-19 associated GI symptoms*
Patient ID	Cases/controls	Age (years)	Sex	Race	Ethnicity	Pertinent medical history/comorbidities §	Indication	Procedure type ‡	Date of procedure	Nasopharyngeal SARS-CoV-2	Duodenum	Ileum		Genomic	Subgenomic						
CGI088	case	32	M	White	Non-hispanic	seasonal allergies, asthma	GERD	EGD/COLO	June 2020	Negative	+	+	+	-	-	March 2020	May 2020	92	94	2	N
CGI089	case	67	M	AA	Non-hispanic	MM, HTN	IDA	EGD/COLO	July 2020	Negative	+	+	N/A	-	-	March 2020	July 2020	N/A	106	2	N
CGI090	case	73	M	White	Hispanic	gout, HTN, prostate Cx	CRC screen, GERD	EGD/COLO	July 2020	Negative	-	-	N/A	-	-	March 2020	N/A	119	112	2	N
CGI091	case	40	F	White	Non-hispanic	asthma	bowel changes	EGD/COLO	July 2020	Negative	-	-	N/A	-	-	N/A	May 2020	N/A	N/A	2	N
CGI092	case	70	M	White	Non-hispanic	HTN, HLD	CRC screen, GERD	EGD/COLO	July 2020	Negative	+	+	N/A	Duodenum	-	April 2020	August 2020	N/A	105	2	Y
CGI093	case	48	F	N/A	Hispanic	fibromyalgia, PUD, IDA, psoriasis	PUD	EGD	July 2020	Negative	-	N/A	N/A	-	-	N/A	May 2020	121	N/A	2	Y
CGI094	case	30	M	White	Non-hispanic	IBD (Crohn)	IBD (Crohn)	EGD/COLO	August 2020	Negative	-	-	N/A	Terminal ileum	-	April 2020	N/A	N/A	113	2	N
CGI095	case	27	F	N/A	Hispanic	allergic rhinitis, GERD	IBS	EGD/COLO	August 2020	Negative	-	-	N/A	-	-	April 2020	N/A	N/A	130	2	N
CGI096	case	63	M	White	Hispanic	prostate Cx, ESRD, DM, HTN	Rectal bleeding	COLO	August 2020	Negative	N/A	-	N/A	-	-	April 2020	N/A	N/A	148	5	N
CGI097	case	28	M	White	Non-hispanic	IBD (Crohn)	IBD (Crohn)	COLO	August 2020	Negative	N/A	-	N/A	-	-	March 2020	June 2020	N/A	99	1	N
CGI098	case	72	F	AA	Non-hispanic	asthma, HTN, HCV	CRC screen	EGD/COLO	September 2020	Negative	-	-	N/A			March 2020	N/A	N/A	166	2	Y
CGI099	case	70	M	AI	Non-hispanic	CRC, IDA, CAD	IDA	COLO	September 2020	Negative	-	-	N/A	Duodenum	Duodenum	N/A	May 2020	173	N/A	2	Y
CGI100	case	30	M	White	Non-hispanic	DM1, CD	CD	EGD	September 2020	Negative	+	N/A	N/A	-	-	N/A	May 2020	N/A	N/A	1	N
CGI106	case	36	M	White	Non-hispanic	seasonal allergies, asthma	abdominal pain, weight loss	EGD	July 2020	Negative	+	N/A	N/A	N/A	N/A	N/A	N/A	N/A	113	2	Y
Ctrl 1	control	79	F	N/A	N/A	anemia, renal angiomyolipoma, breast Cx, DM2, HTN	gastric ulcer follow up	EGD	September 2018	N/A	-	N/A	N/A	N/A	N/A	N/A	N/A	N/A	N/A	N/A	N/A
Ctrl 2	control	79	F	N/A	N/A	Afib, CHF, anemia, HTN, MR	weight loss	EGD	May 2019	N/A	-	N/A	N/A	N/A	N/A	N/A	N/A	N/A	N/A	N/A	N/A
Ctrl 3	control	55	M	N/A	N/A	GERD, EE	abdominal pain	EGD	July 2019	N/A	-	N/A	N/A	N/A	N/A	N/A	N/A	N/A	N/A	N/A	N/A
Ctrl 4	control	83	F	N/A	N/A	asthma, CAD, DM2, HTN, GERD, HLD, OA	dysphagia	EGD	July 2019	N/A	-	N/A	N/A	N/A	N/A	N/A	N/A	N/A	N/A	N/A	N/A
Ctrl 5	control	30	M	N/A	N/A	seasonal allergies, asthma, GERD	GERD	EGD	January 2018	N/A	-	N/A	N/A	N/A	N/A	N/A	N/A	N/A	N/A	N/A	N/A
Ctrl 6	control	51	F	N/A	N/A	ulnar neuropathy, biceps tendonitis	CRC screen	COLO	April 2019	N/A	N/A	-	N/A	N/A	N/A	N/A	N/A	N/A	N/A	N/A	N/A
Ctrl 7	control	57	M	N/A	N/A	GERD, HTN, DM2, migraine, OSA, IBS, diverticulosis	abdominal pain	COLO	April 2019	N/A	N/A	-	N/A	N/A	N/A	N/A	N/A	N/A	N/A	N/A	N/A
Ctrl 8	control	42	M	N/A	N/A	none	rectal bleeding	COLO	September 2019	N/A	N/A	-	N/A	N/A	N/A	N/A	N/A	N/A	N/A	N/A	N/A
Ctrl 9	control	57	M	N/A	N/A	spinal cord injury, paraplegia, HTN, HLD	CRC screen	COLO	October 2019	N/A	N/A	-	N/A	N/A	N/A	N/A	N/A	N/A	N/A	N/A	N/A
Ctrl 10	control	33	M	N/A	N/A	DM2, obesity, HTN, heart murmur	IDA	COLO	October 2019	N/A	N/A	-	N/A	N/A	N/A	N/A	N/A	N/A	N/A	N/A	N/A

AA = African American
AI = Asian Indian
§ = GERD (gastroesophageal reflux disease), CRC (colorectal cancer), IDA (iron deficiency anemia), PUD (peptic ulcer disease), IBD (inflammatory bowel disease), HLD (hyperlipidemia), MV (mitral valve prolapse), MR (mitral regurgitation), DM (diabetes mellitus type 2) OA (osteoarthritis), HTN (arterial hypertension), COPD (chronic obstructive pulmonary disease), CAD (coronary artery disease), Afib (atrial fibriliation), CHF (congestive heart failure), OSA (obstructive sleep apnea), IBS (irritable bowel syndrome), CD (celiac disease), MM (multiple myeloma), ESRD (end stage renal disease), HCV (hepatitis C), EE (eosinophilic esophagitis), MDD (major depressive disorder), Cx (cancer)
‡ EGD = Esophagogastroduodenoscopy; COLO = colonoscopy
¶ = WHO Ordinal Scale for Clinical Improvement; COVID-19 Trial Design Synopsis
† = Persistent fatigue, dyspnea, athletic deficit, or ≥ 3 other solicited symptoms beyond 6 weeks from symptom onset
* GI symptoms at the time of acute illness including diarrhea, nausea, vomiting

799

800 **Supplementary Table 7: Gastrointestinal biopsies cohort characteristics**

801

References

1 Robbiani, D. F. *et al.* Convergent antibody responses to SARS-CoV-2 in convalescent individuals. *Nature* **584**, 437-442, doi:10.1038/s41586-020-2456-9 (2020).

2 Carfi, A., Bernabei, R., Landi, F. & Gemelli Against, C.-P.-A. C. S. G. Persistent Symptoms in Patients After Acute COVID-19. *JAMA* **324**, 603-605, doi:10.1001/jama.2020.12603 (2020).

3 American Medical Association. Long-term Health Consequences of COVID-19. 1-2, doi:10.1001/jama.2020.20677 (2020).

4 Yang, H. S. *et al.* SARS-CoV-2 antibody characterization in emergency department, hospitalized and convalescent patients by two semi-quantitative immunoassays. *Clin Chim Acta* **509**, 117-125, doi:10.1016/j.cca.2020.06.004 (2020).

5 Roche Diagnostics. *Elecsys Anti-SARS-CoV-2*, <https://www.fda.gov/media/137605> (2020).

6 Schmidt, F. *et al.* Measuring SARS-CoV-2 neutralizing antibody activity using pseudotyped and chimeric viruses. *J Exp Med* **217**, 284-218, doi:10.1084/jem.20201181 (2020).

7 Wajnberg, A. *et al.* Robust neutralizing antibodies to SARS-CoV-2 infection persist for months. *Science (New York, N.Y.)*, eabd7728-7727, doi:10.1126/science.abd7728 (2020).

8 Seow, J. *et al.* Longitudinal observation and decline of neutralizing antibody responses in the three months following SARS-CoV-2 infection in humans. *Nat Microbiol*, 1-17, doi:10.1038/s41564-020-00813-8 (2020).

9 Brouwer, P. J. M. *et al.* Potent neutralizing antibodies from COVID-19 patients define multiple targets of vulnerability. *Science (New York, N.Y.)* **369**, 643-650, doi:10.1126/science.abc5902 (2020).

10 Cao, Y. *et al.* Potent Neutralizing Antibodies against SARS-CoV-2 Identified by High-Throughput Single-Cell Sequencing of Convalescent Patients' B Cells. *Cell* **182**, 73-84 e16, doi:10.1016/j.cell.2020.05.025 (2020).

11 Ju, B. *et al.* Human neutralizing antibodies elicited by SARS-CoV-2 infection. *Nature* **584**, 115-119, doi:10.1038/s41586-020-2380-z (2020).

12 Kreer, C. *et al.* Longitudinal Isolation of Potent Near-Germline SARS-CoV-2-Neutralizing Antibodies from COVID-19 Patients. *Cell* **182**, 843-854 e812, doi:10.1016/j.cell.2020.06.044 (2020).

13 Seydoux, E. *et al.* Analysis of a SARS-CoV-2-Infected Individual Reveals Development of Potent Neutralizing Antibodies with Limited Somatic Mutation. *Immunity* **53**, 98-105 e105, doi:10.1016/j.immuni.2020.06.001 (2020).

14 Yuan, M. *et al.* Structural basis of a shared antibody response to SARS-CoV-2. *Science (New York, N.Y.)* **369**, 1119-1123, doi:10.1126/science.abd2321 (2020).

15 Weisblum, Y. *et al.* Escape from neutralizing antibodies by SARS-CoV-2 spike protein variants. *Elife* **9**, doi:10.7554/eLife.61312 (2020).

16 Barnes, C. O. *et al.* SARS-CoV-2 neutralizing antibody structures inform therapeutic strategies. *Nature*, 1-25, doi:10.1038/s41586-020-2852-1 (2020).

17 Tortorici, M. A. *et al.* Ultrapotent human antibodies protect against SARS-CoV-2 challenge via multiple mechanisms. *Science (New York, N.Y.)* **4**, eabe3354-3316, doi:10.1126/science.abe3354 (2020).

18 Baum, A. *et al.* Antibody cocktail to SARS-CoV-2 spike protein prevents rapid mutational escape seen with individual antibodies. *Science (New York, N.Y.)* **369**, 1014-1018, doi:10.1126/science.abd0831 (2020).

19 Li, Q. *et al.* The Impact of Mutations in SARS-CoV-2 Spike on Viral Infectivity and Antigenicity. *Cell* **182**, 1284-1294 e1289, doi:10.1016/j.cell.2020.07.012 (2020).

20 Lamers, M. M. *et al.* SARS-CoV-2 productively infects human gut enterocytes. *Science (New York, N.Y.)* **369**, 50-54, doi:10.1126/science.abc1669 (2020).

21 Livanos, A. E. *et al.* Gastrointestinal involvement attenuates COVID-19 severity and mortality. *medRxiv*, 1-52, doi:10.1101/2020.09.07.20187666 (2020).

22 Qian, Q. *et al.* Direct evidence of active SARS-CoV-2 replication in the intestine. *Clin Infect Dis*, 1-6, doi:10.1093/cid/ciaa925 (2020).

23 Han, Y. *et al.* Identification of SARS-CoV-2 Inhibitors using Lung and Colonic Organoids. *Nature*, doi:10.1038/s41586-020-2901-9 (2020).

24 Morone, G. *et al.* Incidence and Persistence of Viral Shedding in COVID-19 Post-acute Patients With Negativized Pharyngeal Swab: A Systematic Review. *Front Med (Lausanne)* **7**, 562, doi:10.3389/fmed.2020.00562 (2020).

25 Park, S. K. *et al.* Detection of SARS-CoV-2 in Fecal Samples From Patients With Asymptomatic and Mild COVID-19 in Korea. *Clin Gastroenterol Hepatol*, 1-11, doi:10.1016/j.cgh.2020.06.005 (2020).

26 Wolfel, R. *et al.* Virological assessment of hospitalized patients with COVID-2019. *Nature* **581**, 465-469, doi:10.1038/s41586-020-2196-x (2020).

27 Beaudoin-Bussieres, G. *et al.* Decline of Humoral Responses against SARS-CoV-2 Spike in Convalescent Individuals. *mBio* **11**, 398-397, doi:10.1128/mBio.02590-20 (2020).

28 Crawford, K. H. D. *et al.* Dynamics of neutralizing antibody titers in the months after SARS-CoV-2 infection. *J Infect Dis*, 1-15, doi:10.1093/infdis/jiaa618 (2020).

29 Iyer, A. S. *et al.* Persistence and decay of human antibody responses to the receptor binding domain of SARS-CoV-2 spike protein in COVID-19 patients. *Sci Immunol* **5**, eabe0367-0313, doi:10.1126/sciimmunol.abe0367 (2020).

30 Wang, K. *et al.* Longitudinal dynamics of the neutralizing antibody response to SARS-CoV-2 infection. *Clin Infect Dis* **579**, 270-279, doi:10.1093/cid/ciaa1143 (2020).

31 Muecksch, F. *et al.* Longitudinal analysis of serology and neutralizing antibody levels in COVID19 convalescents. *The Journal of Infectious Diseases*, doi:10.1093/infdis/jiaa659 (2020).

32 Schafer, A. *et al.* Antibody potency, effector function and combinations in protection from SARS-CoV-2 infection in vivo. *bioRxiv* **182**, 828-826, doi:10.1101/2020.09.15.298067 (2020).

33 Ripperger, T. J. *et al.* Orthogonal SARS-CoV-2 Serological Assays Enable Surveillance of Low Prevalence Communities and Reveal Durable Humoral Immunity. *Immunity*, 1-49, doi:10.1016/j.immuni.2020.10.004 (2020).

34 Liu, L. *et al.* Potent neutralizing antibodies against multiple epitopes on SARS-CoV-2 spike. *Nature* **584**, 450-456, doi:10.1038/s41586-020-2571-7 (2020).

35 Zost, S. J. *et al.* Potently neutralizing and protective human antibodies against SARS-CoV-2. *Nature* **584**, 443-449, doi:10.1038/s41586-020-2548-6 (2020).

36 Nielsen, S. C. A. *et al.* Human B Cell Clonal Expansion and Convergent Antibody Responses to SARS-CoV-2. *Cell host & microbe* **28**, 516-525 e515, doi:10.1016/j.chom.2020.09.002 (2020).

37 Kaneko, N. *et al.* Loss of Bcl-6-Expressing T Follicular Helper Cells and Germinal Centers in COVID-19. *Cell* **183**, 143-157 e113, doi:10.1016/j.cell.2020.08.025 (2020).

38 Victora, G. D. & Nussenzweig, M. C. Germinal centers. *Annu Rev Immunol* **30**, 429-457, doi:10.1146/annurev-immunol-020711-075032 (2012).

39 Mahler, D. A. & Wells, C. K. Evaluation of clinical methods for rating dyspnea. *Chest* **93**, 580-586, doi:10.1378/chest.93.3.580 (1988).

40 Pujadas, E. *et al.* SARS-CoV-2 viral load predicts COVID-19 mortality. *The Lancet. Respiratory medicine* **8**, e70, doi:10.1016/S2213-2600(20)30354-4 (2020).

41 Chomczynski, P. & Sacchi, N. Single-step method of RNA isolation by acid guanidinium thiocyanate-phenol-chloroform extraction. *Analytical biochemistry* **162**, 156-159, doi:10.1006/abio.1987.9999 (1987).

42 DeAngelis, M. M., Wang, D. G. & Hawkins, T. L. Solid-phase reversible immobilization for the isolation of PCR products. *Nucleic Acids Res* **23**, 4742-4743, doi:10.1093/nar/23.22.4742 (1995).

43 Grifoni, A. *et al.* Targets of T Cell Responses to SARS-CoV-2 Coronavirus in Humans with COVID-19 Disease and Unexposed Individuals. *Cell* **181**, 1489-1501 e1415, doi:10.1016/j.cell.2020.05.015 (2020).

44 Amanat, F. *et al.* A serological assay to detect SARS-CoV-2 seroconversion in humans. *Nat Med* **26**, 1033-1036, doi:10.1038/s41591-020-0913-5 (2020).

45 Barnes, C. O. *et al.* Structures of Human Antibodies Bound to SARS-CoV-2 Spike Reveal Common Epitopes and Recurrent Features of Antibodies. *Cell* **182**, 828-842 e816, doi:10.1016/j.cell.2020.06.025 (2020).

46 Schmidt, F. *et al.* Measuring SARS-CoV-2 neutralizing antibody activity using pseudotyped and chimeric viruses. *J Exp Med* **217**, doi:10.1084/jem.20201181 (2020).

47 Weisblum, Y. *et al.* Escape from neutralizing antibodies by SARS-CoV-2 spike protein variants. *bioRxiv* **17**, 1055-1042, doi:10.1101/2020.07.21.214759 (2020).

48 Gupta, N. T. *et al.* Change-O: a toolkit for analyzing large-scale B cell immunoglobulin repertoire sequencing data. *Bioinformatics (Oxford, England)* **31**, 3356-3358, doi:10.1093/bioinformatics/btv359 (2015).

49 Soto, C. *et al.* High frequency of shared clonotypes in human B cell receptor repertoires. *Nature* **566**, 398-402, doi:10.1038/s41586-019-0934-8 (2019).

50 Guo, Y., Chen, K., Kwong, P. D., Shapiro, L. & Sheng, Z. cAb-Rep: A Database of Curated Antibody Repertoires for Exploring Antibody Diversity and Predicting Antibody Prevalence. *Front Immunol* **10**, 2365, doi:10.3389/fimmu.2019.02365 (2019).

51 Kyte, J. & Doolittle, R. F. A simple method for displaying the hydropathic character of a protein. *J Mol Biol* **157**, 105-132, doi:10.1016/0022-2836(82)90515-0 (1982).

52 Guy, H. R. Amino acid side-chain partition energies and distribution of residues in soluble proteins. *Biophysical journal* **47**, 61-70, doi:10.1016/S0006-3495(85)83877-7 (1985).

53 DeWitt, W. S. *et al.* A Public Database of Memory and Naive B-Cell Receptor Sequences. *PLoS One* **11**, e0160853, doi:10.1371/journal.pone.0160853 (2016).

54 Spiegel, M. *et al.* Inhibition of Beta interferon induction by severe acute respiratory syndrome coronavirus suggests a two-step model for activation of interferon regulatory factor 3. *J Virol* **79**, 2079-2086, doi:10.1128/JVI.79.4.2079-2086.2005 (2005).

55 Mastronarde, D. N. Automated electron microscope tomography using robust prediction of specimen movements. *J Struct Biol* **152**, 36-51 (2005).

56 Mastronarde, D. N. & Held, S. R. Automated tilt series alignment and tomographic reconstruction in IMOD. *J Struct Biol* **197**, 102-113, doi:10.1016/j.jsb.2016.07.011 (2017).

57 Mastronarde, D. N. Correction for non-perpendicularity of beam and tilt axis in tomographic reconstructions with the IMOD package. *Journal of microscopy* **230**, 212-217, doi:10.1111/j.1365-2818.2008.01977.x (2008).

58 Yao, H. *et al.* Molecular Architecture of the SARS-CoV-2 Virus. *Cell*, doi:10.1016/j.cell.2020.09.018 (2020).

59 Ke, Z. *et al.* Structures and distributions of SARS-CoV-2 spike proteins on intact virions. *Nature*, doi:10.1038/s41586-020-2665-2 (2020).

60 Klein, S. *et al.* SARS-CoV-2 structure and replication characterized by in situ cryo-electron tomography. *bioRxiv*, doi:10.1101/2020.06.23.167064v2 (2020).

61 Turoňová, B. *et al.* In situ structural analysis of SARS-CoV-2 spike reveals flexibility mediated by three hinges. *Science* **370**, 203-208, doi:10.1126/science.abd5223 (2020).